Use Authorization

In presenting this thesis in partial fulfillment of the requirements for an advanced degree at Idaho State University, I agree that the library shall make it freely available for inspection. I further state that permission to download and/or print my thesis for scholarly purposes may be granted by the Dean of the Graduate School, Dean of my academic division, or by the University Librarian. It is understood that any copying or publication of this thesis for financial gain shall not be allowed without my written permission.

Signature _____

Date _____

Sensitivity and Uncertainty Analysis in the Homogenization of the EBR-II Core

by
Ryan Stewart

A thesis
submitted in partial fulfillment
of the requirements for the degree of
Master of Science in Nuclear Science and Engineering
Idaho State University
Spring 2017

To the Graduate Faculty:

The members of the committee appointed to examine the thesis of Ryan Stewart find it satisfactory and recommend that it be accepted

_____
Dr. Chad Pope
Major Advisor

_____
Dr. George Imel
Committee Member

_____
Dr. Christopher McGrath
Graduate Faculty Representative

ACKNOWLEDGEMENTS

Throughout this process, there were many people who helped me get to this point in my life and I would like to take the time to quickly thank them.

First and foremost, I would like to thank my wife, Erika, who has been supportive during this entire process. Her countless hours of reading and rereading this paper got me to where I am today. Along with that, her endless support when I get engulfed in my work is greatly appreciated.

I would also like to thank the EBR-II benchmark team for accepting me into their project in the final year and having patience with me as I learned the material. Specifically, I would like to thank Dr. Chad Pope for his willingness to pick up and add me to his already busy schedule. I am greatly appreciative of your willingness to invite me into your research group. I would also like to thank Edward Lum for his tireless effort in helping me understand MICKA and putting in time to help me finish my thesis. Finally, I would like to thank Dr. Chris McGrath for his help in finding me a new research group and his continued support during my transition.

Table of Contents

List of Figures

List of Tables

List of Equations

Abstract

The research for this master's thesis is focused on the creation of a homogenized model of the Experimental Breeder Reactor II (EBR-II) core. The purpose of this research is to determine the viability of homogenization and its applicability for inclusion as a reactor physics benchmark for the International Reactor Physics Experiment Evaluation Project (IRPhEP) handbook. Throughout this process, the EBR-II core was homogenized from the outside working towards the core region to determine the change to k_{eff} and the control rod worth. This thesis presents the homogenization of the blanket region, reflector region, dummy drivers, half-worth drivers, and driver subassemblies. To ensure the process was providing reliable results which corresponded with the underlying physics, a sensitivity analysis was performed on a driver subassembly for both a heterogeneous and homogeneous model. This ensures that if there are changes in k_{eff}, the shifts were not caused by cross-sectional importance, but were due to the material change in the homogenization process. This sensitivity analysis also provides confidence that the homogenization process is applicable for the EBR-II core.

1.0 Introduction

1.1 Background of the Experimental Breeder Reactor II

The Experimental Breeder Reactor II (EBR-II) was a sodium-cooled liquid metal fast reactor (LMFR) which has its roots dating back to the mid to late 1940's, when nuclear science was shifting from weapons design and development to the peaceful use of nuclear energy. It was during this time Enrico Fermi, Leo Szilard, Eugene Wigner, and Alvin Weinberg gathered together to discuss the possibilities of utilizing nuclear energy to operate power plants for the public [1]. During this era, fissile material was scarce and it was decided that a civilian power plant needed to optimize the fissile content. It would also need to produce more fuel than it consumed for continual operation. This idea was the basis for a three-stage reactor design. First, a prototype reactor was built to prove the feasibility of breeding; the first stage culminated in the creation of EBR-I by Argonne National Laboratory (ANL). EBR-I started operation in late 1951, and was a sodium-potassium cooled LMFR, which provided proof in early 1952 that the reactor was breeding more fuel than it was consuming [1]. After the success of EBR-I, the second stage was to test the feasibility of breeding as a fuel source. This stage allowed for the creation of EBR-II. EBR-II operated from 1964 until 1994, where it not only provided the necessary evidence for the feasibility of breeding, but it also provided a valuable research tool for additional projects. The third stage of reactor design was to engage with the nuclear industry and have a full-scale power plant built, deemed EBR-III, along with the necessary reprocessing facilities to allow for a closed fuel cycle. Although EBR-III was never

built, EBR-II provided an extremely useful research tool for LMFR testing and design throughout the approximately 30 years it operated.

EBR-II underwent four main phases of research during its 30 years of operation. The first research stage was meant to pick up where EBR-I left off, and prove an LMFR could breed additional reactor fuel and reprocess the fuel on-site to be used again in the reactor. The next research phase was utilizing EBR-II as an irradiation facility for LMFR fuels and materials testing. This included irradiating different fuel, cladding, and reactor instruments for future use in LMFRs. The third stage was to provide proof of the inherent safety features an LMFR provides by utilizing sodium as a coolant. The last phase was the inclusion of EBR-II in the integral fast reactor development program. The integral fast reactor program was designed to help improve the economics and enhanced safety features of LMFRs [2]. Figure 1 shows the approximate breakdown of research phases for EBR-II.

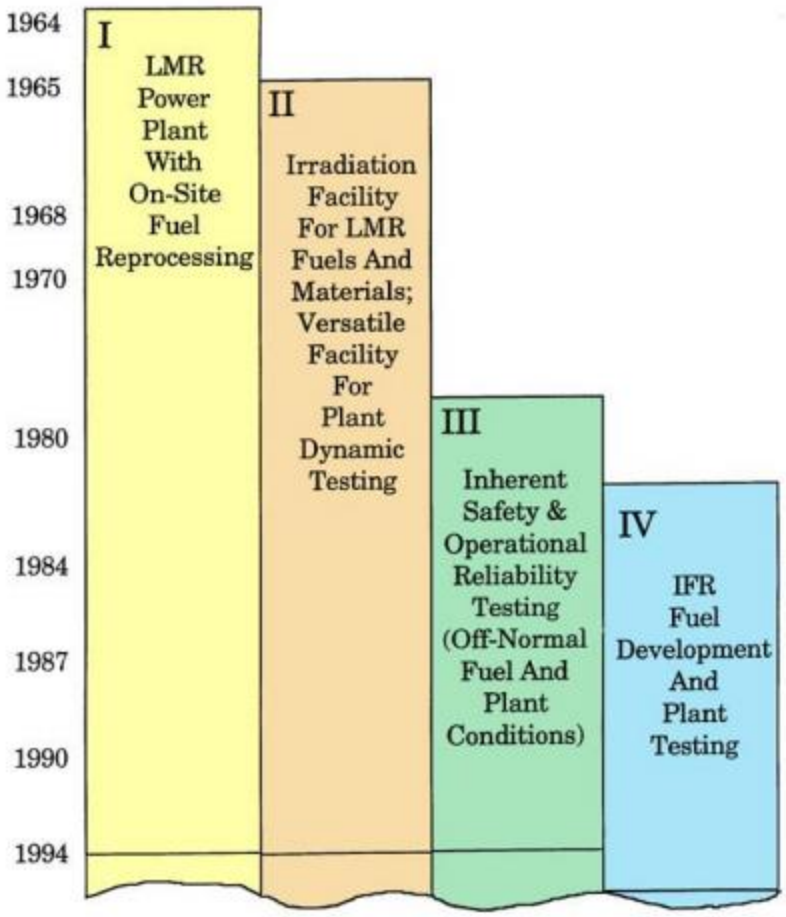

Figure 1. Research phases for EBR-II [3].

The initial design behind EBR-II focused on proving a plant could operate on a closed fuel cycle and maintain operations for the lifetime of the facility. EBR-II went dry critical (critical without sodium coolant) in mid-1960 and wet critical in mid-1964 [4]. Throughout the next few years, the reactor power was taken from between 1.0-5.0 MWth to the full design power of 62.5 MWth, which was achieved in 1969 [4]. Throughout the 1960's, EBR-II's main goal was to provide proof a breeder could produce excess fuel, and fuel could then be reprocessed and utilized in the same reactor while it operated as a power station. During the 1970's, the fuel recycling facility was shut down; however, EBR-II operated as a power plant for ANL and provided an irradiation facility for LMFR materials. Beginning in the 1980's, EBR-II

focused on the inherent safety features LMFR's provide by testing accident conditions for future LMFRs. During this period the safety heat removal tests (SHRT) were performed, which were designed to test a LMFRs ability to cope with a catastrophic failure of heat removal systems at full power. This stage of research provided information which would later aid in the development of the Integral Fast Reactor (IFR) program [5]. The development of IFR looked to take the lessons learned from EBR-II, and incorporate them into a similar reactor design.

1.2 Safety Heat Removal Test

During the 1980's, EBR-II was utilized to test how an LMFR would react to a failure of the heat removal system at full power. The specific experiments which tested these conditions were known as Safety Heat Removal Tests (SHRT). Their purpose was to prove EBR-II had inherent safety features that enabled it to shut itself down without significant core damage. Of the dozens of SHRT experiments, the most intensive experiment was SHRT 45 during run 138B, conducted on April 3rd, 1986 [3]. This experiment disabled the reactor automatic SCRAM mechanism while simultaneously running down the primary and secondary cooling pumps. With the SCRAM disabled, the control rods were at a critical configuration with all being fully inserted (fueled control rods pulled to a height of 14.0 cm), except three high worth control rods (of which two were fully withdrawn, and one was raised 3.01 cm) [6]. The experiment simulated a station wide blackout with the addition of no ability to SCRAM the reactor.

The SHRT experiment started with EBR-II at its full rated 62.5 MW power when the circuit breaker for the primary and secondary pumps was tripped, which lead to both pumps coasting down [3]. The auxiliary pump, which controlled the sodium flow to the ambient heat

exchanger, was operational due to the fact it operates on a battery pack given a blackout. SHRT 45 encompassed the worst-case scenario given a station blackout, while the other SHRT experiments tested aspects of this scenario as detailed in Table 1.

Table 1. Plant Conditions for SHRT 40, 41, and 45 [3]

SHRT No.	Initial Power (% of rated)	Initial primary flow (% of rated)	Initial secondary flow (% of normal)	Primary pump coast down condition	Auxiliary pump condition	Secondary pump coast down condition
40	50	100	68	Passively controlled, 95s	On battery	Trip of 2400V breaker to M-G set
41	50	100	68	Actively controlled, 200s	Off	Same as SHRT 40
45	100	100	100	Passively controlled, 200s	On	Same as SHRT 40

As predicted, the peak fuel temperature in EBR-II rose slightly after the initial trip, and then steadily reduced in temperature due the ability to passively remove heat from the reactor core. After the experiment was conducted, analysis showed there was no detectable fuel breach as a result of the experiment, and there was only minimal thermal stress damage to the fuel [3]. EBR-II was able to restart without any significant complications, and the test was a success in showing LMFRs could withstand potential catastrophic failures without major core damage. Due to the success of this experiment and the implications it has on future LMFR design, it was decided to focus on run 138B as a benchmark analysis for the International Reactor Physics Experiment Evaluation Project (IRPhEP) handbook.

1.3 Benchmark Evaluation Project

The IRPhEP handbook started in 1999 and was created for the international reactor physics community as a tool for reactor designers and safety analysts, and to aid in the validation of new calculational techniques and data [7]. To perform this task the IRPhEP focuses on gathering, characterizing, and simulating reactor physics experiments throughout the world. The handbook aids the international community by consolidating and preserving information that already exists, and aims to help retrieve lost data or find where additional data is needed. Along with this, the handbooks aim is to find discrepancies between calculations and experiments due to deficiencies, eliminate redundant research on reactor physics experimental data, and improve future experimental planning, execution, and reporting [7].

The EBR-II benchmark evaluation project was initially investigated by Dr. Chad Pope at Idaho State University. Since the project's conception, there have been two master's theses produced, a handful of undergraduate research projects, and there are currently two doctoral candidates with projects involving the benchmark evaluation. The overview for the project is to produce a reactor physics benchmark evaluation for run 138B which will be included in the IRPhEP handbook. To fulfill this project, a model of the reactor core during run 138B was required. It was decided Monte Carlo N-Particle (MCNP) would be utilized to model the EBR-II core at the time of run 138B [8]. This model incorporated the entire EBR-II core and was created based on the engineering diagrams from EBR-II. These designs incorporated known uncertainties in both materials and dimensions. To determine if run 138B is an acceptable benchmark, the simulated results must provide a value for criticality in accordance with the known values. Once the simulated results are obtained, perturbations must be applied to account for the given uncertainties in the design. To be eligible for a benchmark, these

perturbations must provide values for criticality which are near the original simulated results and will provide an overall uncertainty which is meaningful.

There were over 150 perturbations needed to provide enough information for the benchmark project. Each perturbation would require a new input file. Given the complexity of the input file, a MATLAB code was created by Edward Lum to assist in the creation of MCNP input files. The program is called the MCNP Input Card & Kcode Architect (MICKA).

1.4 MICKA

MICKA was created by for a twofold purpose. The first was to create an extremely detailed model of the EBR-II reactor. This model was meant to be detailed to provide as accurate of a representation of EBR-II as possible. Despite this goal, it was necessary in some aspects to simplify the model due to the enormous complexities of the EBR-II core. The second goal for MICKA is to allow for small perturbations to be made in the detailed core with relative ease. MICKA allows user inputs to determine which perturbations will be made, and creates a new input file to reflect these changes. These changes can vary from material, to temperature, to dimensional perturbations. Had MICKA not been utilized, it would have taken hours to create each input file given the smallest perturbation, thus MICKA provides the framework for producing the MCNP benchmark input files with relative ease.

Despite the great attributes MICKA provides, it also comes with drawbacks. MICKA, in its current iteration, is approximately 15,000 lines of code. This is an extremely large code to manage, and it requires an intimate knowledge of the program to alter even the simplest lines without causing a disruption in the rest of the code. The benchmark input file MIKCA creates for MCNP is also extremely detailed, and takes considerable time to run. Each input file is

approximately 130,000 lines, and each requires long runtimes to produce reliable results given the extreme complexity in the geometry. Although this level of detail is required for the benchmark analysis, the average user would likely find the MCNP benchmark input files created of little use when trying to compare reactor designs of a similar nature. For use in a comparison, it was found a simpler model would provide adequate detail without needing the intimate knowledge of MICKA or having the extreme detail of the MCNP file it produces.

1.5 Simplified Model

Early in the benchmark project construction, it was determined a simplified model would be required due to the extreme complexity of the benchmark input file. The simplified model solved this issue by applying various techniques to simplify the geometry and material composition of the core, while still maintaining an accurate neutronic representation of what was occurring in the EBR-II core. To simplify the model, MICKA was altered to apply cell averaging techniques and homogenize many of the dimensions and materials. This homogenization provides a simple input file, which can be used for future fast reactor analysis. This future analysis could utilize the general EBR-II core layout, with the ability to quickly alter the materials and dimensions for separate work. To determine the effectiveness and the applicability of the homogenization techniques, a sensitivity and uncertainty analysis was

performed on a heterogeneous and homogeneous driver subassembly to determine how homogenization affected the neutronics.

2.0 Literature Review

2.1 Fast Reactor Physics

To understand the homogenization process, it is important to understand the physics occurring in the EBR-II core. Fast reactors have unique nuclear characteristics which invalidate many of the assumptions used in thermal reactor analysis. For example, due to neutrons having a long mean free path in a fast reactor, the core is coupled and must be examined on a more global basis [9]. Due to this, it is important to address the unique characteristics of a fast reactor core. EBR-II is considered a fast reactor due to the neutron flux spectrum of the reactor being in the intermediate and high neutron energy regimes. Intermediate neutron energies are between 0.625 eV to 100 keV, and fast neutrons are anything greater than 100 keV. This meant nearly all of the fissions occurring in the core were due to fast or intermediate neutrons. The driving force behind this was the ability of the coolant to elastically scatter neutrons without significantly decreasing the energy. The energy an isotope can absorb from a neutron can be described by the logarithmic energy decrement per collision, seen in Equation 1, where α is described in Equation 2, and A is the atomic mass number of the isotope [10].

$$\xi = 1 + \frac{\alpha}{1-\alpha} ln(\alpha)$$

Equation 1

$$\alpha = \left(\frac{A-1}{A+1}\right)^2$$

Equation 2

Many of the materials in EBR-II had large elastic scattering cross-sections, but few had the slowing-down power hydrogen has in a typical light water reactor [9]. The slowing down power of an element is the product of the average logarithmic energy decrement and the macroscopic elastic cross section. Table 2 compares the slowing-down properties of materials in EBR-II.

Table 2. Slowing-Down Properties of Major Constituent Materials for EBR-II (adapted from Yang)

	Scattering Cross Section (b)	Atom Density (/b*cm)	Slowing-down Power (cm^{-1})
TRU	4.0	5.19E-5	1.78E-6
U	5.6	2.74E-2	1.32E-3
Zr	8.1	7.56E-4	1.34E-3
Fe	3.4	5.66E-2	6.85E-3
Na	3.8	2.25E-2	7.41E-3
H*	11.9	2.90E-2	3.5E-1

*Typical values in a pressurized water reactor

Table 2 shows the slowing-down power of any one material in a typical sodium fast reactor is at most around 2% of what hydrogen is in a light water reactor. From this, a neutron is more likely to leak out or be absorbed before it reaches thermal energies. Although the neutrons do not reach thermal energies, the elastic scattering does result in a neutron energy spectrum in the keV to MeV range, with few energies less than 1 keV [9]. This results in a neutron being born and inducing fission in similar energy ranges.

2.2 Homogenization

The homogenization process requires a detailed knowledge of the reactor core, and a theoretical understanding of the implications of homogenization. To examine the effect of homogenization, it is important to understand some conceptual reactor physics; namely the six factor formula. Although the six factor formula does not accurately describe a reactor on a process level, it is helpful to provide a basic intuition into the physics occurring in the background, and can be used to describe how effectively a reactor multiplies neutrons in a given core. The mathematical form is given in Equation 3.

$$k = \eta_{th} f p \epsilon P_{FNL} P_{TNL}$$

Equation 3

In this equation, η_{th} is the average number of neutrons produced per absorption in the fuel; f (thermal utilization factor) is the probability a neutron absorbed in the reactor gets absorbed in the fuel; p is the fraction of neutrons that escape absorption in the resonance region; ϵ is the fraction of fission caused by fast neutrons; P_{FNL} is the probability a fast neutron will not leak out; P_{TNL} is the probability a thermal neutron will not leak out [11]. Again, it is important to note the six factor formula was created for thermal reactors, but it will still provide insight into a fast reactor like EBR-II.

In a homogenous core, the fuel and coolant are thoroughly mixed together. In a heterogeneous core, the fuel and coolant are all modeled individually. The most dramatic difference from changing a heterogeneous core to a homogeneous core is the decrease in the resonance escape probability. From a heuristic standpoint, this occurs because neutrons that are born in a heterogeneous fuel pin and leak out have a greater opportunity to scatter and lose energy in the

coolant [11]. In a homogenous mixture, the fuel and coolant are one. As a neutron scatters, it has a higher probability of being absorbed in the resonance escape region, due to there being no separation between the fuel and coolant. This effect of heterogeneous cells is known as resonance self-shielding, and is extremely important when considering a thermal reactor system due to a highly non-uniform distribution of the neutron flux. In a LMFR, the affect is not as dramatic despite a majority of the neutron flux being in the epithermal and fast energy spectrum. This damped effect is due to a nearly flat spatial distribution of the energy spectra in the core due to the long mean free path of these neutrons [12]. Therefore, the homogenization process should not have as pronounced an effect on the EBR-II core as it would on a thermal core.

Fast fission is negatively influenced by homogenization. When neutrons are born in a heterogeneous fuel pin at high energies, they have the potential to cause additional fission neutrons before they leak out into the coolant [11]. When the coolant and the fuel are homogenized, there is a higher probability the neutron will encounter some type of moderating material, which will decrease its energy before finding a fissionable nucleus to cause a fission [13].

EBR-II is a fast spectrum reactor, which will greatly reduce the importance of the thermal utilization factor. Nearly all of the fissions occurring will be in the keV to MeV range, and thus the thermal utilization factor is replaced with the fuel utilization factor, which encompasses fuel utilization over the entire energy spectrum.

In a typical reactor the thermal fission factor, η_{th}, is the ratio between the absorption and fission cross section in the fuel, given by Equation 4 [11].

$$\eta_{th} = \frac{\nu\sigma_f^F}{\sigma_a^F} = \sum_j \frac{\nu_j \Sigma_f^j}{\Sigma_a^j}$$

Equation 4

This ratio is appreciably affected by homogenization. This effect comes from the change in the ratio of absorptions. The incident energies utilized are dependent on the spectrum, which is in turn dependent on position in a heterogeneous fuel pin lattice. When homogenization occurs, it increases the energy spectrum of the incident neutrons, which decreases the probability of absorption in the fuel. This decrease is due to the fuel and moderator being in the same material and having roughly equivalent absorption cross-sections, however the moderator has a higher atom density. In this case, if the fuel and moderator have the same cross-sectional area, then the moderator has a higher probability of absorption than the fuel.

Along with the six factor formula, it is important to consider lattice effects in the homogenization process. The fast neutron mean free path is typically much larger than the lattice dimensions, which prevents interference with the fast non-leakage factor when homogenization is taken into consideration. For a LMFR, the neutron flux for any energy group will typically have an almost flat spatial distribution, except near boundary boundaries [12]. This distribution is due to the long mean free path for fast neutrons. This flat spatial distribution allows for a unit cell consisting of fuel, cladding, and coolant to easily be homogenized into a one-unit cell. This homogenization technique of combining the fuel, cladding, and coolant is common practice and can be found in work by the NEA and OECD [14].

Having a fast-neutron spectrum greatly reduces the impact of homogenization, but does not altogether eliminate its effects. Along with this, utilizing a continuous energy cross-section set greatly reduces the initial input needed by the user for the homogenization process. The

homogenization technique for a multi-group energy problem requires the user to have a firm understanding of the effects homogenization will have on the system. A multi-group approach must take into account resonance characteristics of many nuclides and self-shielding effects in fissile and fertile nuclides [9]. This requires both heterogeneous and homogeneous calculations in a two-dimensional system and acquiring the appropriate neutron-energy flux weighting factors [15]. The energy-dependent weighting factors then allow for a more appropriate treatment of the homogenized system. With a continuous-energy cross-section set, this step can be by-passed in favor of having a more thorough cross-section set, which does not require specific weight functions. One of the drawbacks of utilizing continuous-energy cross-section sets for analyzing the homogenization process is the calculation time [16].

Despite the gains from utilizing continuous cross-section sets, there are still areas which in the resonance region which can affect the homogenization process. With neutron energies greater than ~1 keV, some resonances are wide enough to prevent detecting a single resonance, and instead multiple resonances blend together [16]. When this occurs, additional methods are used to represent the resonance structure of cross sections; averaged cross-sections, statistical distributions of resonance parameters, and the resonance ladder method [16]. These methods were not examined in the scope of the homogenization process, but could provide valuable information for future work.

The case for homogenization altering k_{eff} is best described by examining the effect on the first man made reactor, Chicago Pile 1 (CP-1). During the creation of CP-1, the significance of self-shielding was investigated by Enrico Fermi and Leo Szilard, and it was determined to be imperative to separate the natural uranium fuel slugs and place graphite between them [17]. This separation allowed adequate time for the neutrons to slow down and reach thermal

energies to cause fission in the fuel. If the fuel and graphite had been homogenized into one material, CP-1 would have never gone critical due to the fact that CP-1 ran on natural uranium.

2.3 Sensitivity Analysis

Sensitivity analysis was pioneered by ANL and has been around for decades, but has recently become a major tool in Monte Carlo reactor analysis due to the increase in computational abilities. The software package, SCALE, comes with a built in sensitivity analysis tool called the Tools for Sensitivity and UNcertainty Analysis Methodology Implementation (TSUNAMI) [18]. TSUNAMI was utilized to compute sensitivity and uncertainty data for material compositions. To understand the resulting data, a quick introduction is provided for direct first-order perturbation for a Monte Carlo process.

TSUNAMI has been used in previous EBR-II analysis for pyroprocessing of spent EBR-II fuel, in the electrorefiner. For pyroprocessing, TSUNAMI was utilized to analyze an abnormal event which would dictate the amount of fuel dissolved in the electrorefiner [19]. This case examined if the anode and cathode were to reverse roles, and if actinides in the salt accumulated on the fuel dissolution basket [19]. The role reversal simulation was run in SCALE, utilizing TSUNAMI, and results provided quantitative results that the most reactive anode/cathode dominated k_{eff}. For a fast system, the salts used in the elecrorefiner (lithium, potassium and chlorine) have smaller sensitivities in comparison to the fissionable nuclides [19]. These results are important when examining an EBR-II driver subassembly, where the subassembly will be dominated by the fissionable material content, despite having close to the same volume as the sodium coolant.

Sensitivity analysis stems from the basics of perturbation theory, and thus a brief introduction of perturbation theory is presented. Perturbation theory stems from making small changes to core geometry or composition to elicit a response in k_{eff} without having to recalculate k_{eff}. There are multiple methods used to interrogate the sensitivities; among them are the direct perturbation, adjoint flux, and iterative fission probability.

For a direct perturbation, a general sensitivity parameter $S_{k,Nj}$ is defined as a response of k_{eff} to the atom density of N_j. In a first order perturbation, the atom density of N_j is increased and decreased from the nominal value by a percentage which will generate a statistically significant response in k_{eff} [20]. The sensitivity parameter is defined in Equation 5, where 0 is the initial unperturbed value for k_{eff} and the j^{th} nuclide, and the + and – are results of the direct perturbation [21].

$$S_{k,N_j} = \frac{N_{j,0}}{k_0} * \frac{\partial k}{\partial N_j} = \frac{N_{j,0}}{k_0} * \frac{k_{N_j}{}^{+} - k_{N_j}{}^{-}}{N_j{}^{+} - N_j{}^{-}}$$

Equation 5

The sensitivity parameter indicates the effect each isotope, N_j, will have on k_{eff} for the system. This sensitivity is the product of three independent Monte Carlo calculations, all of which have statistical uncertainties. These uncertainties are propagated to the uncertainties in the direct perturbation sensitivity coefficient. It is assumed these uncertainties are not correlated, which allows for the use of standard error propagation techniques resulting in Equation 6 [22].

$$\sigma_s = \left(\left(\frac{\left(\sigma_{k^+}^2 + \sigma_{k^-}^2\right)}{(k^+ + k^-)^2} + \frac{\sigma_k^2}{k_0^2} \right) * \left(\frac{k^+ + k^-}{k_0} \right)^2 \right)^{\frac{1}{2}} * \left(\frac{N_{j,0}}{N_j{}^+ - N_j{}^-} \right)$$

Equation 6

Favorite et al. show a detailed description of how the sensitivity of the j[th] nuclide's atom density is equal to the sensitivity of the mass density (ρ_j) of the j[th] nuclide [21]. In addition to this, they show the sensitivities of individual atoms or mass densities can be summed to create the total atom or mass density sensitivities. The ability to sum the sensitivities only pertains to first-order sensitivities. Higher-order sensitivities are not additive, and this method is not applicable. The results of the atom and mass density equivalence are shown in Equation 7.

$$S_{k,N} = \sum_{j=1}^{J} S_{k,N_j} = \sum_{j=1}^{J} S_{k,\rho_j} = S_{k,\rho}$$

Equation 7

The result from Equation 7 can also be extended to the macroscopic cross section Σ_t [21]. This means a sensitivity response to a material atom density change is the exact same as the response to the total macroscopic cross section [20]. Overall, the direct perturbation is simple to perform for a Monte Carlo simulation as it requires a base model and the adjustment of a parameter to determine the impact it has on k_{eff}. The drawback is the need to run multiple simulations for each parameter perturbed, which is inefficient. To alleviate running multiple simulations, it is common to use first-order perturbation theory.

In multi-group perturbation theory, the flux (also called forward flux) and adjoint flux (neutron importance) of the original system are required before calculating any perturbations to the system. Once the forward and adjoint flux are found, first order perturbation theory can be used to perturb different parameters in the system to find the change in k_{eff}, and the parameters

sensitivity coefficient. This method only requires one simulation to be run but it requires multi-group cross section sets, which causes multiple difficulties in the homogenization process. To alleviate the multi-group cross section sets, the IFP method can be used.

The iterative fission probability (IFP) method with continuous energy cross sections was selected for the sensitivity analysis in the homogenization process. This method stores the reaction rates of neutrons for a particular number of generations until an asymptotic population of their descendants are reached in the system. The asymptotic population is then used to weight the reaction rates for the particular neutrons to determine the sensitivity coefficients. The generations skipped, or latent generations, ensure an asymptotic population is reached before utilizing the asymptotic population to weight the reaction rates. For both the heterogeneous and homogeneous models, five latent generations were skipped [23]. The iterative fission probability method is represented in Figure 2.

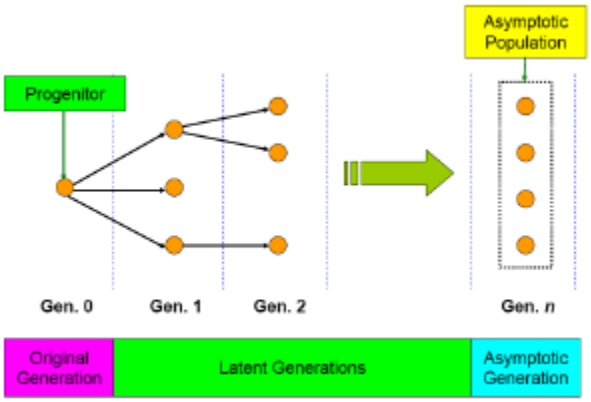

Figure 2. The iterative fission probability method [18].

It is important to note that the IFP method calculates the importance of a particle directly as it is tracked through the system. Utilizing the IFP method means the adjoint flux is not required to calculate the sensitivities of nuclides in the system. The drawback of utilizing the IFP method is the increase in calculation time relative to the direct, or adjoint calculations, and the

large amount of memory required. For the analysis of EBR-II, the IFP method was chosen for its use of continuous energy cross section sets to alleviate the burden that comes with multi-group cross-sections, and the decrease in time to calculate multiple perturbations.

Despite the power and versatility of TSUNAMI, it is important to realize the analysts' selection of modeling techniques within TSUNAMI can impact the results [24]. For example, errors in the implicit sensitivity coefficients can be caused if cross-section resonance self-shielding is inconsistent with the materials used [20]. The use of continuous energy cross-section sets is meant to help alleviate this with the ability to calculate importance particle importance without calculating the adjoint flux. Despite this, it is important for the analyst to perform a direct set of perturbations to ensure the accuracy of the TSUNAMI sensitivity data.

2.4 Monte Carlo

MCNP is a stochastic Monte Carlo particle transport code which incorporates pointwise continuous energy cross sections, generalized geometry, and time-dependence. It can be used to determine the neutron flux, as well as k_{eff} eigenvalues for fissile systems. The process by which a neutron transports through the system can be described by using Monte Carlo theory along with random numbers. In a given multiplying system, a neutron is originally born, either out of fission or a starting neutron, and it requires three pieces of information. First, the neutron requires its location, which is specified by the user, or is the position of a previous fission. Secondly, a direction is required to determine where the neutron will go; the process of choosing the neutron's direction takes two random numbers. The neutron now has a direction, but needs an energy. For a neutron born out of fission, the energy is found by using four random numbers, which are required to sample a Watt fission spectrum. To determine how far a

neutron will travel before a collision, one random number is used to generate the macroscopic transport cross section. At this point, the neutron has now used seven random numbers.

The seven random numbers provide the neutron with a direction, a speed at which it is traveling, and how far, on average, it will travel before colliding with something. Given this information, there are three possibilities. First, the neutron can leak out of the system; if it did, that neutron is no longer tracked, and a new neutron will need to be generated. Second, the neutron can enter a region with a different material composition; if so, a new macroscopic transport cross section will need to be produced. Finally, a neutron can have a collision; if so, the isotope collided with will need to be determined. The isotope selection is based on the atom densities for the region, and a neutron interacts with an isotope depending on the random number selected. Given the direction, energy, and isotope being collided with, the next step is to find which type of reaction occurs. This process is similar to the atom densities, and is based on the size of the cross section. A random number is again used to determine the reaction occurring. This process took nine random numbers to determine one neutron traversing through the media and interacting with one isotope.

When the neutron interacts with an isotope, there are a few possibilities which are dependent on what reaction occurs. First, a neutron can scatter; if a scatter occurs, a new energy and direction are chosen, and the neutron continues. Second, a neutron is can be absorbed; if it is absorbed, either parasitic capture or a fission can occur. If a neutron is parasitically captured, it is lost to the system and a new neutron is produced at a fission site in the system. If a neutron causes a fission, a random number is used to determine how many neutrons are produced, which is dependent on the fissile isotope. Figure 3 shows the analog Monte Carlo neutron tracking process, described in detail above.

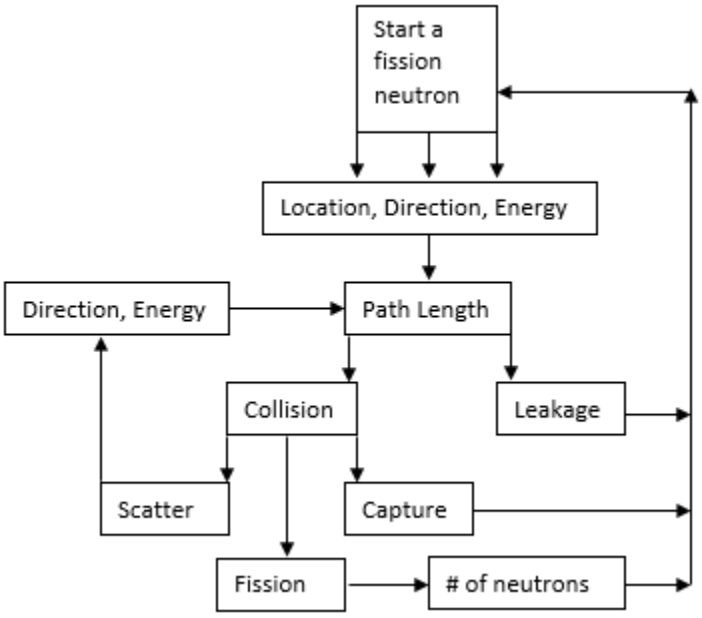

Figure 3. MCNP analog neutron tracking.

Due to the extreme detail in the MCNP models created for EBR-II, it was essential to introduce some variance reduction techniques to reduce the run time and increase the efficiency of sampling. For example, if a neutron is parasitically captured, a variance reduction technique called survival biasing is placed into effect. This process is slightly different from the analog Monte Carlo process described above, where the neutron would just be absorbed and a new neutron would need to be tracked. To prevent wasted particles, survival biasing allows the neutron to continue on after being absorbed, but it loses some of its weight. When a neutrons weight becomes extremely small, Russian roulette is played with the particle. A random number is selected, and if it is greater than some threshold set, the neutron will be killed and no longer tracked. If the number is lower than the threshold, it will increase its weight based on the threshold value and continue being tracked. This process prevents a neutron being tracked for an extremely long period of time just to be lost to a

parasitic absorption. This technique is widely used, and is the MCNP default for particle tracking.

3.0 Benchmark Data

3.1 Detailed Description of the EBR-II Core

EBR-II was a pool-type sodium cooled fast breeder reactor loaded with a uranium metal fuel, and later a uranium-plutonium fuel [4]. Figure 4 and Figure 5 show detailed diagrams of the EBR-II primary system and the EBR-II core.

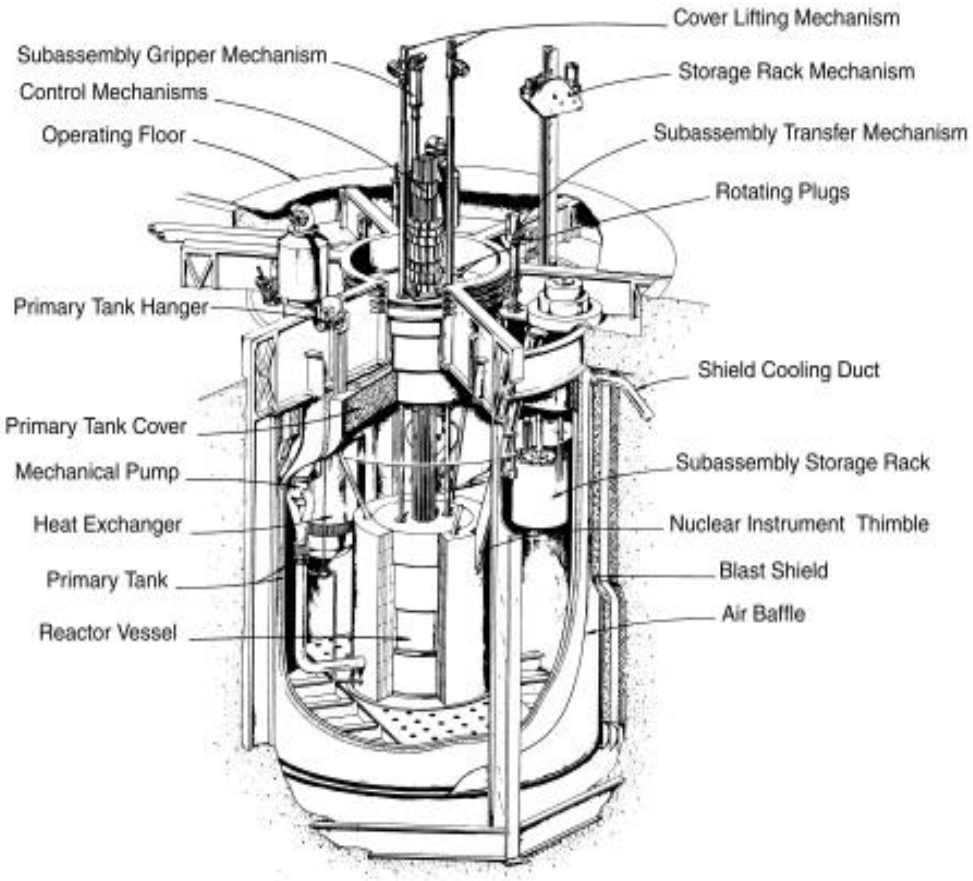

Figure 4. Detailed layout of the primary coolant system [4].

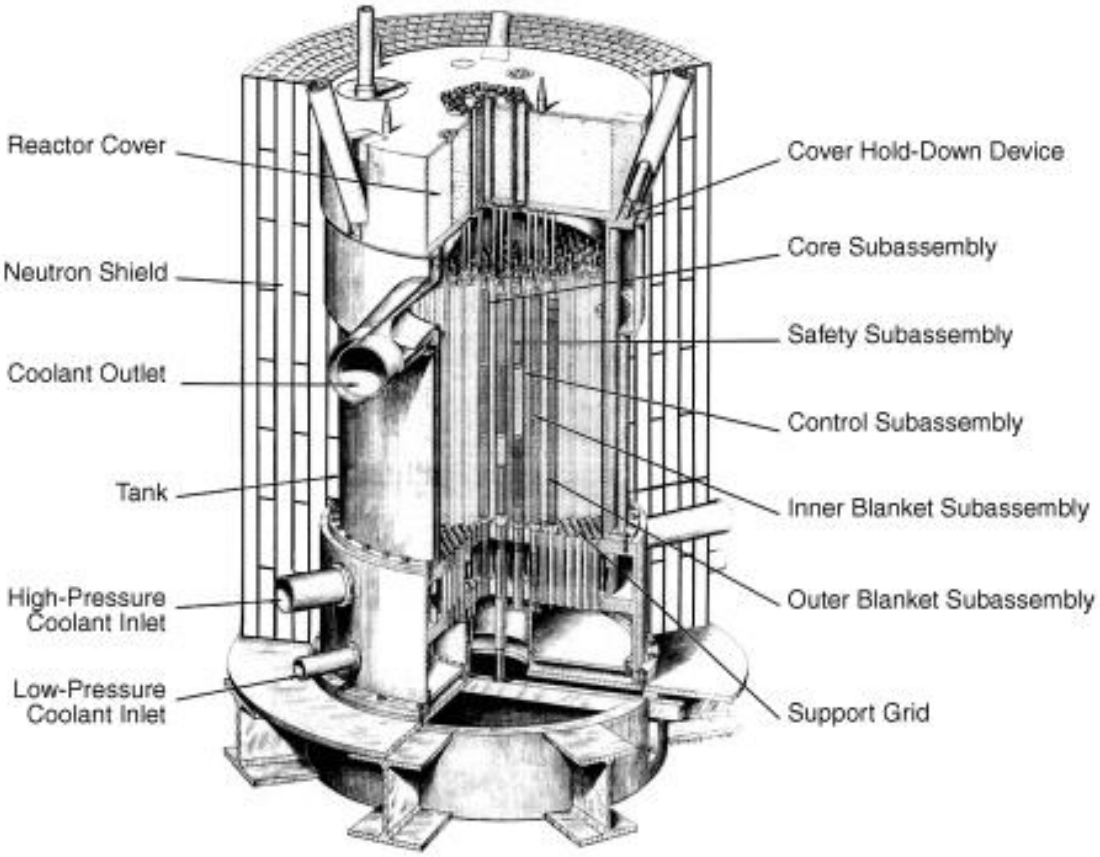

Figure 5. Design layout of the EBR-II core [4].

Intermediate heat exchangers were located in the primary pool, to extract heat away from the core to be used for steam production. The fuel was highly enriched uranium metal, approximately 67 wt%. The metal uranium fuel has a large thermal expansion and high thermal conductivity, which contribute to EBR-II's inherent safety features [4]. The metal fuel and pool-type design allowed the core to be cooled by passive sodium convection in the event of a catastrophic failure, as demonstrated by the SHRT tests. The core design was hexagonal with an assembly pitch of 5.89 cm. The effective core height was 34.29 cm, and the effective core diameter was 69.67 cm. The core was split into 637 hexagonal subassemblies, which were made up of eight different types of subassemblies. The reactor core is divided into three main regions: core, inner blanket, and outer blanket.

Subassembly locations were denoted by three parameters: row, section, and position within the core. If a horizontal slice of the core was taken, the central subassembly would be row 1. Row 2 follows with six subassemblies immediately surrounding row 1. Row 3 and on follow the same pattern, with each row growing by six until the row 14 of the core is reached. The last two rows, 15 and 16, have 66 and 24 subassemblies, respectively. The core is then split into six sections labeled A through F. A line is drawn from the central assembly and through each assembly towards the outside edge, in approximately 60 degree angles, which split the core evenly. A subassembly position is determined by the number of subassemblies from each line of the six sectors. For example, position 05C04 contains a driver subassembly. To find it on the map, the third section (which corresponds to C) is selected. This is followed by moving up five subassemblies on the 120-degree line, starting with the central subassembly. This will be subassembly 05C01; then move to the right four subassemblies starting with 05C01. The designator on the map is 2777A, and is highlighted in Figure 6, which shows the core layout and the subassembly position scheme for the core region.

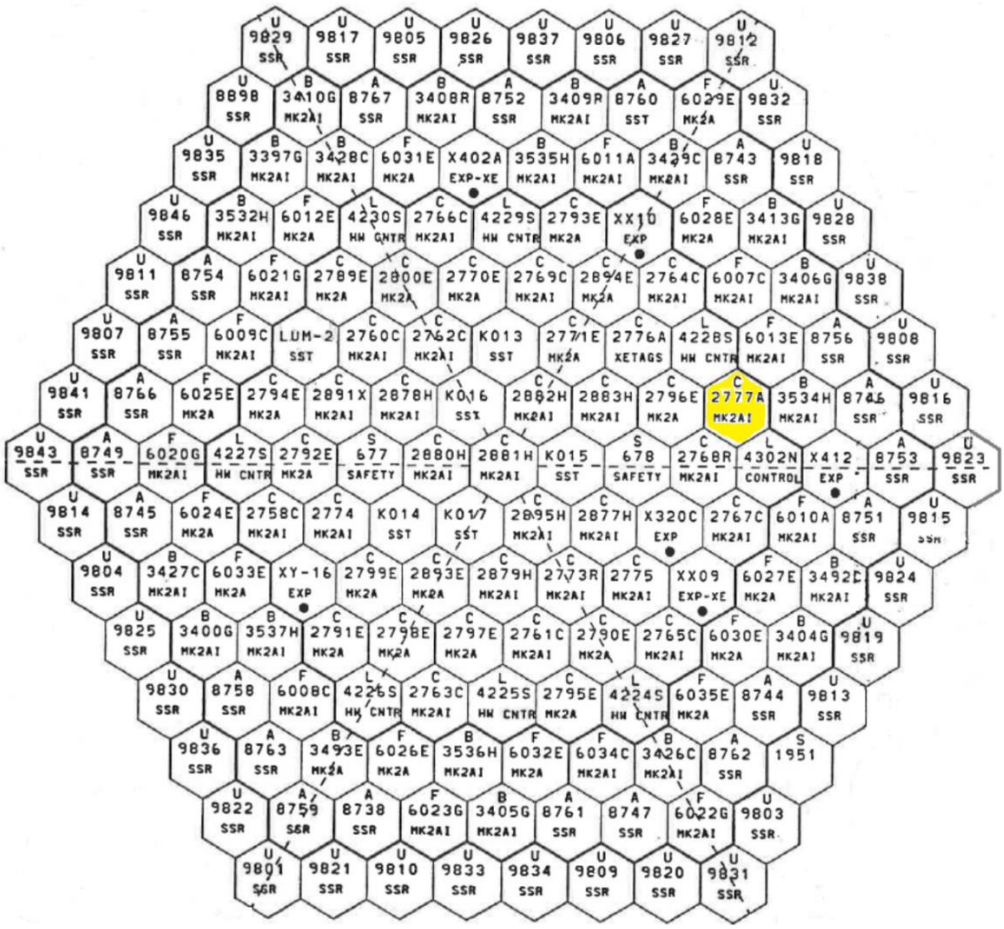

Figure 6. Core layout and the subassembly position scheme [25].

The core region of EBR-II originally encompassed the first five rows, and contains 61 subassemblies. For run 138B, the core region included row 6, and contained seven control rod subassemblies; two in row 3, and five in row 5, along with three instrumented test subassemblies, also in row 5. The remainder of the core was driver fuel or experimental-irradiation subassemblies. Row 7 contained the stainless steel reflector, while rows 8 through 16 contained 510 subassemblies of either blanket or stainless steel reflector subassemblies. Figure 7 shows a diagram of the EBR-II core for run 138B.

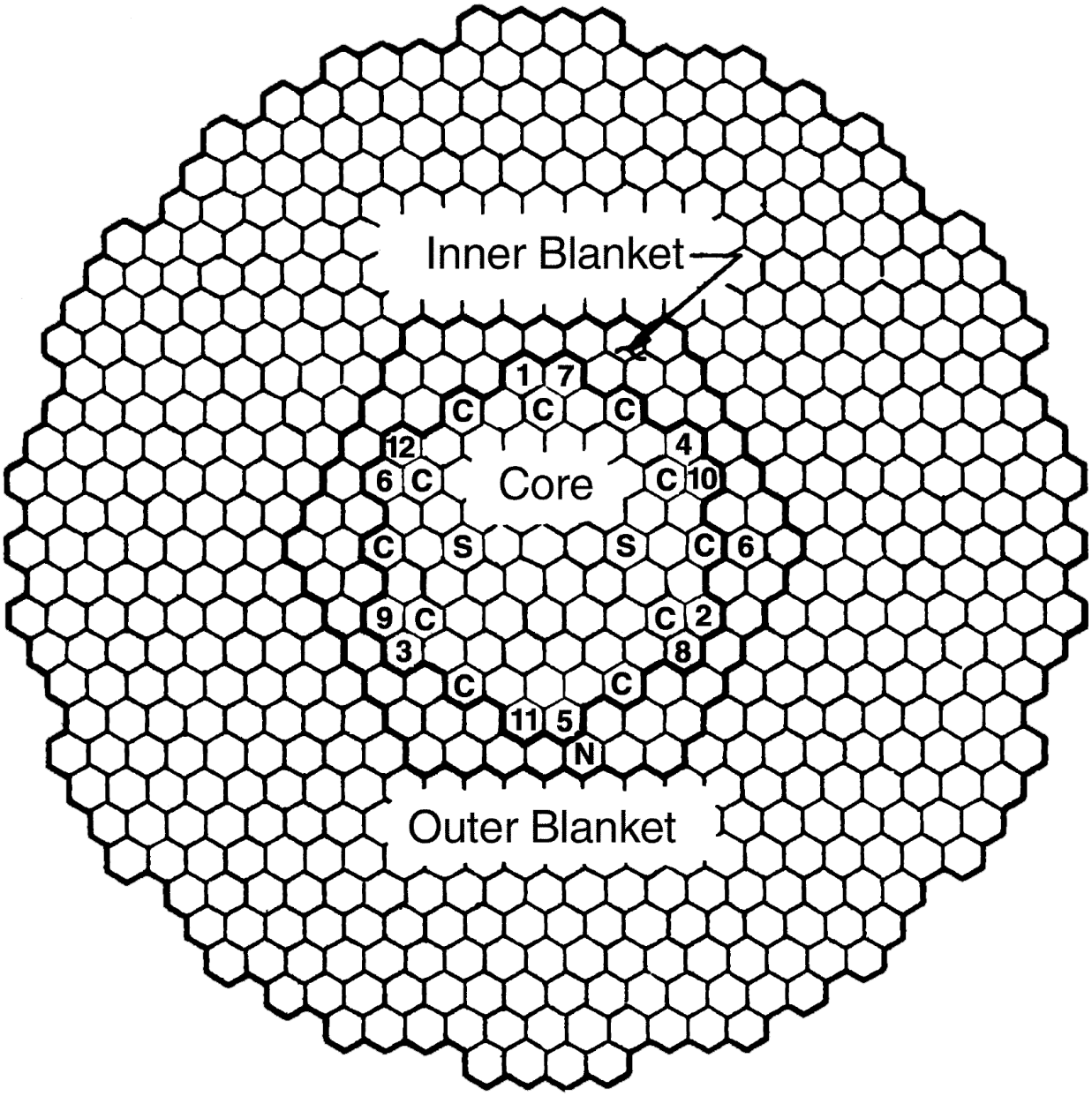

Figure 7. Full core layout of EBR-II [26].

During run 138B, multiple types of subassemblies were utilized: driver, dummy, control, safety, experimental, reflector, and blanket. The driver subassemblies were MARK-IIA (MKIIA), MARK-II AI (MKIIAI), or MARK-IIS (MKIIS) depending on when they were manufactured. From these driver types, variations were created for several purposes. Half-worth drivers were made by removing half of the fuel elements and replacing them with

stainless steel dummy rods. High-flow drivers were identical to a standard driver, except for extra flow holes drilled in the inlet nozzle to allow for a higher coolant flow. These drivers were typically in areas of the core with a higher neutron flux. Dummy subassemblies contained no fuel, and in its place contained only stainless steel rods. The safety and control subassemblies were movable driver subassemblies, whereas high worth control subassemblies were movable driver subassemblies that contained a boron carbide section above the fuel. Run 138B contained four experimental drivers, which were utilized for instrumentation during the run. Reflector subassemblies contained stainless steel, whereas blanket subassemblies contained depleted uranium.

3.2 Dimensional and Material Descriptions for Subassemblies

Each subassembly had a similar structural design. A subassembly contained a lower adapter which connected with the reactor grid plate, and determined the amount of coolant flow through the subassembly. The coolant flow rate was based upon the size of the nozzle drilled through the lower adapter. The central region contained a hexagonal outer duct, which protected the inner region and channeled the coolant through the subassembly. The last region in each subassembly was the upper pole piece, which was utilized to properly orient the subassembly within the reactor by allowing a moving mechanism to attach to the upper pole piece and place it into the core. The upper pole piece was not modeled in any of the subassemblies due to its negligible impact on k_{eff}. The basic design of the subassemblies was

maintained throughout each type, however, the subassemblies position in the core and type of subassembly determines the specific characteristics.

For Figure 8 through Figure 16 the color scheme depicts the materials present in the subassembly. In general, hot pink denotes the sodium coolant, orange or light pink depicts the lower adapter, teal denotes the smeared lower and upper extension, yellow denotes the hex duct, and bright green denotes the stainless-steel dummy pin. The fuel slugs for both driver and blanket fuel pins are split into three regions and each has a different color.

3.2.1 Detailed Description for Subassemblies in MICKA

The driver subassemblies consisted of all five parts of a typical subassembly. The lower adapter was a homogenization of stainless steel 304 (SS304) and sodium, and was modeled as a cylinder with a diameter of 4.76 cm. It was used to place the subassembly into the reactor grid plate. The lower extension was the first part of the subassembly, which was enclosed in the hexagonal duct. The hexagonal duct had an internal flat-to-flat distance of 5.61 cm, and an outer flat-to-flat distance of 5.82 cm. The lower extension was 61.35 cm in height and was designed to allow for sodium flow from the lower adapter in addition to being an axial reflector for the fueled regions. This section was immensely difficult to model due to the complexities of the sodium flow streams, and it was decided a smear of 88.4 wt% SS316 and 11.6 wt% sodium would be sufficient. The fueled region was contained in the hexagonal duct and contained 91 fuel pins. The fuel pins were arranged in a hexagonal lattice with a triangular pitch of 0.57 cm, and will be discussed later. The upper extension was similar to the lower extension in design. It allowed coolant to flow from the fueled region, within the hexagonal duct, to the upper pole piece, and provided axial reflection for the fueled section. The upper

extension was modeled as a smear of 90.29 wt% SS316 and 9.71 wt% sodium, and was 40.60 cm in height. The upper pole piece was not modeled. Figure 8 shows a driver subassembly, as modeled in MICKA.

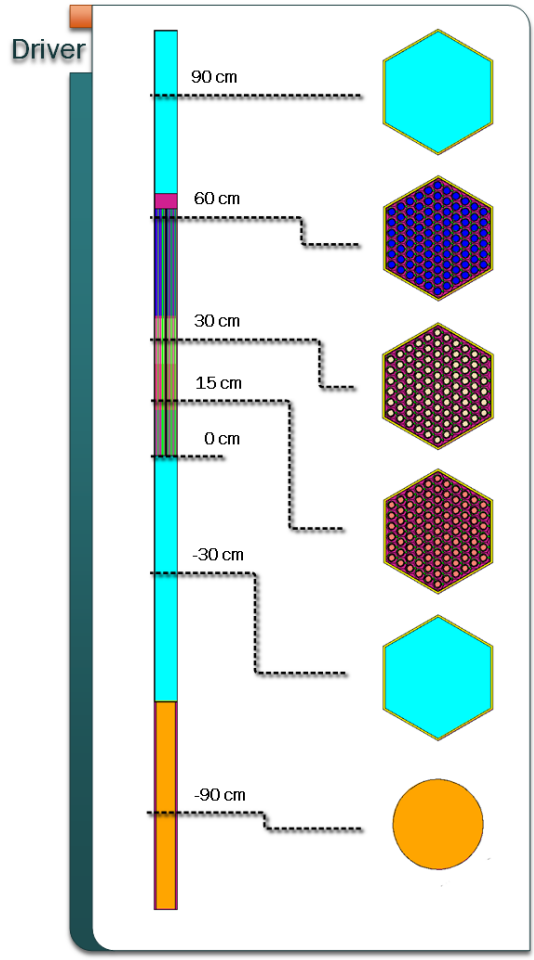

Figure 8. MCNP plot of driver subassembly [26].

Half-worth drivers were identical to core drivers with the exception that 45 of the fuel pins were SS304 dummy pins while the other 46 were fully fueled pins. Figure 9 shows a half-worth driver subassembly.

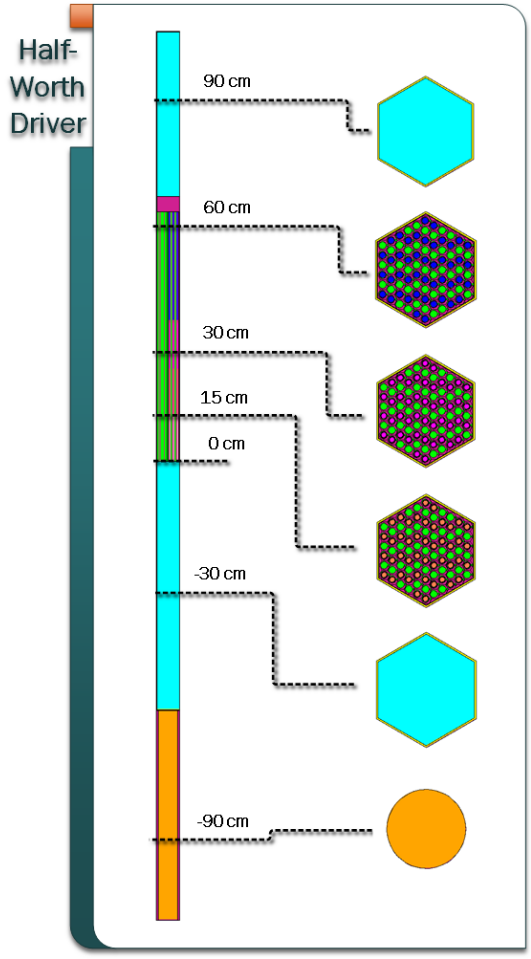

Figure 9. MCNP plot of half-worth driver subassembly [26].

Stainless steel dummy subassemblies consisted of only two parts, a lower adapter, and a hexagonal duct with seven SS304L (a slightly different alloy of SS304) or SS316 (dependent upon core placement) dummy pins running nearly the full length of the duct. The duct was 167.12 cm long, and was made of SS304L or SS316. The dummy pins were 145.28 cm tall with a diameter of 2.04 cm and a triangular pitch of 2.05 cm. Figure 10 shows a stainless steel dummy subassembly.

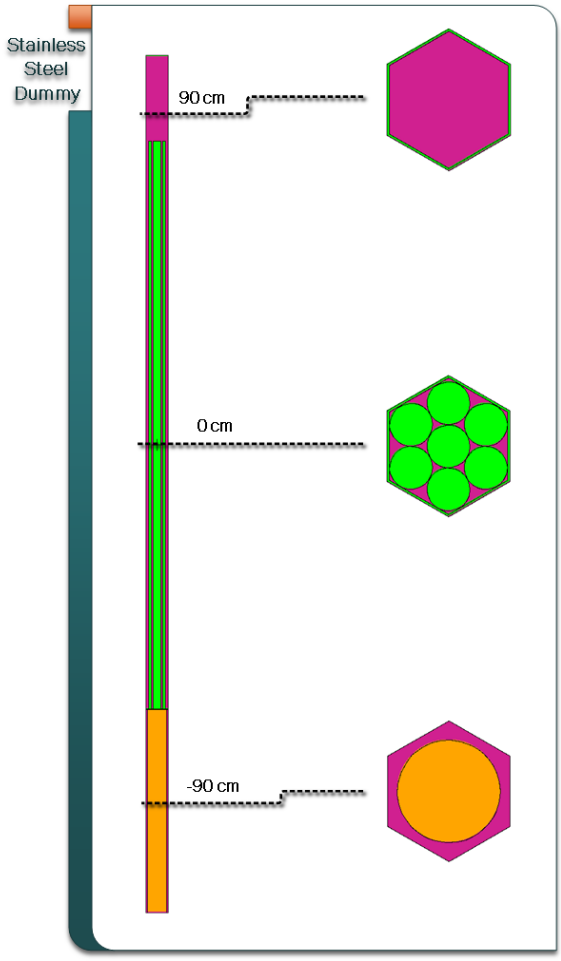

Figure 10. MCNP plot of dummy subassembly [26].

The reflector subassemblies were very similar to the stainless steel subassemblies, with the major difference being hexagonally stacked blocks, which were modeled as one long block which was homogenized with the sodium bond surrounding it. The lower adapter was 52.07 cm tall and 4.91 cm in diameter. The blocks ran the entire length of the subassembly and were either made of SS304 or SS316 homogenized with sodium, depending on core placement. The hexagonal block had a flat-to-flat distance of 5.82 cm, and were 167.02 cm in total height. The hexagonal duct had an inner flat-to-flat diameter identical to the hexagonal block flat-to-flat diameter and an outer flat-to-flat diameter of 5.82 cm. Where the bright yellow is the stainless

steel block section, and the remainder of the color scheme is consistent. Figure 11 shows a reflector subassembly.

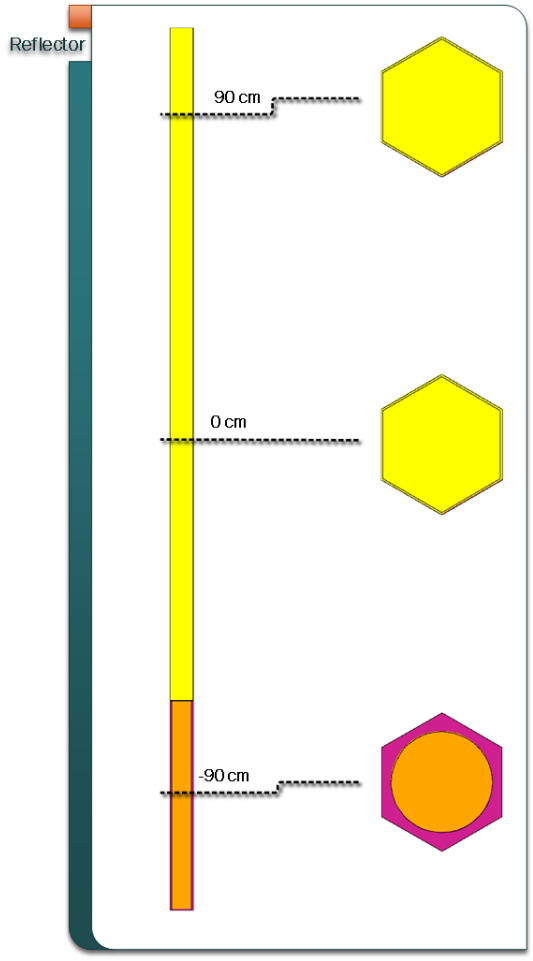

Figure 11. MCNP plot of stainless steel reflector subassembly [26].

The outer blanket subassemblies had a lower adapter with a height of 52.07 cm, and a diameter of 3.83 cm. This was followed by the blanket region, which contained 19 blanket fuel pins with a triangular pitch of 1.26 cm in a hexagonal duct. The height of the blanket region was 155.58 cm. Figure 12 shows an outer blanket subassembly.

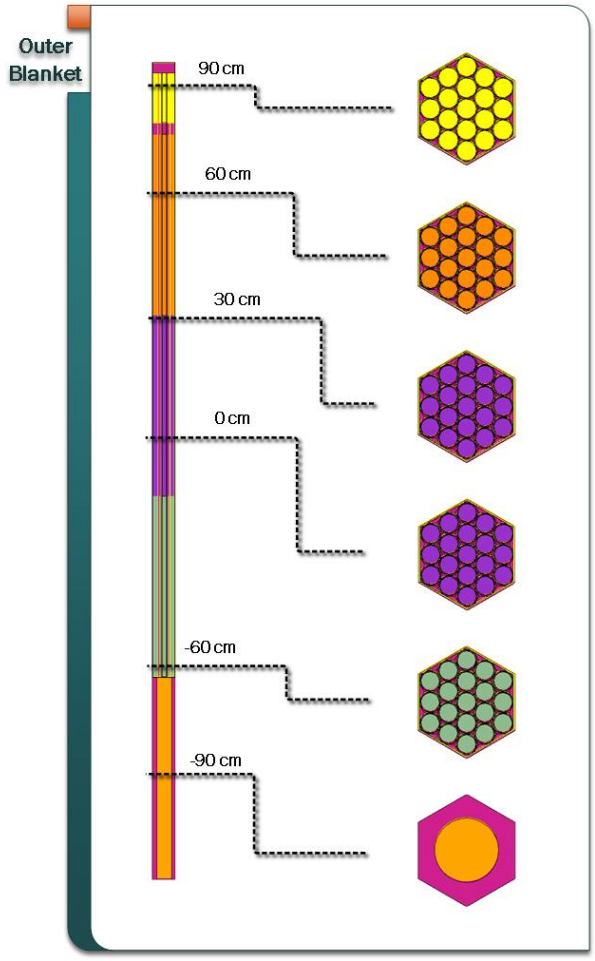

Figure 12. MCNP plot of blanket subassembly [26].

The safety subassemblies were designed as movable driver subassemblies, with a smaller fuel loading. The safety subassembly was the same size as a driver subassembly, however, it had a movable inner hexagonal duct inside of the subassembly. The inner duct had an inner flat-to-flat diameter of 4.83 cm and an outer diameter of 4.90 cm. The inner duct could move up to 35.56 cm into the core. The lower adapter held the subassembly and moved the entire subassembly through the core. The lower adapter was again modeled as a cylinder with a height of 82.63 cm, and a diameter of 4.907 cm and can be seen in light pink. The lower extension served both as a sodium channel and as an axial reflector, exactly like the driver fuel. The lower extension was made of 88.40 wt% SS316 and 11.60 wt% sodium. This section had a

height of 61.75 cm and can be seen in light pink. The fuel element region contained 61 MKIIA fuel pins arranged with a triangular pitch of 0.57 cm and had a height of 66.66 cm, which again, each slug section had different colors. The upper extension served as a sodium channel and an axial reflector for the fueled region and can be seen in teal. It had a height of 37.30 cm, and was modeled as a 90.29 wt% SS and 9.71 wt% sodium smear. The outer hexagonal duct had a flat-to-flat inner diameter of 5.82 cm and outer diameter of 5.89 cm, along with a height of 103.27 cm. Figure 13 shows a safety subassembly.

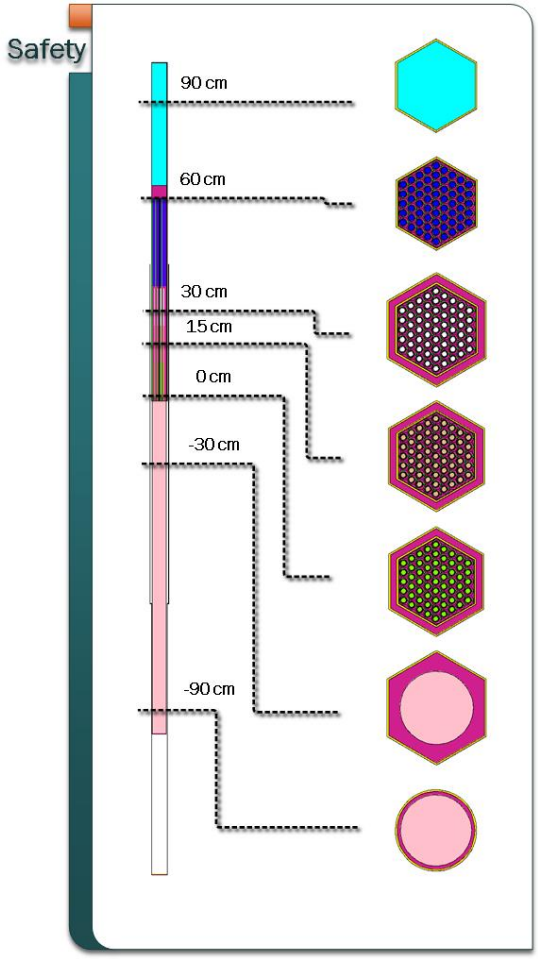

Figure 13. MCNP plot of a safety subassembly [26].

The high worth control subassemblies were similar to the safety subassemblies. They utilized a smaller fuel loading, 61 fuel pins, along with the inner hexagonal ducts ability to move. The

difference between safety and high worth control subassemblies was that the high worth control subassemblies have an extra section dedicated to the poison pins. The lower adapter had a height of 71.98 cm and a diameter of 4.91 cm. The lower extension had a height of 52.23 cm, with a 88.40 wt% SS and a 11.60 wt% sodium smear. The core region was 51.56 cm in height, and contained 61 MKIIS fuel elements with a triangular lattice of 0.57 cm. Above the fueled region was an upper extension which contained B_4C poison pins in addition to a stainless steel and sodium upper extension. The B_4C pins were almost directly above the fueled region, and contained seven poison pins with a pitch of 1.59 cm. The poison pins were 1.59 cm in diameter and 91.67 cm in height, and can be seen in dull pink and bright green. Above the poison pins was the upper extension with a height of 66.55 cm, containing 90.29 wt% SS and 9.71 wt% sodium. Figure 14 shows a high worth control subassembly.

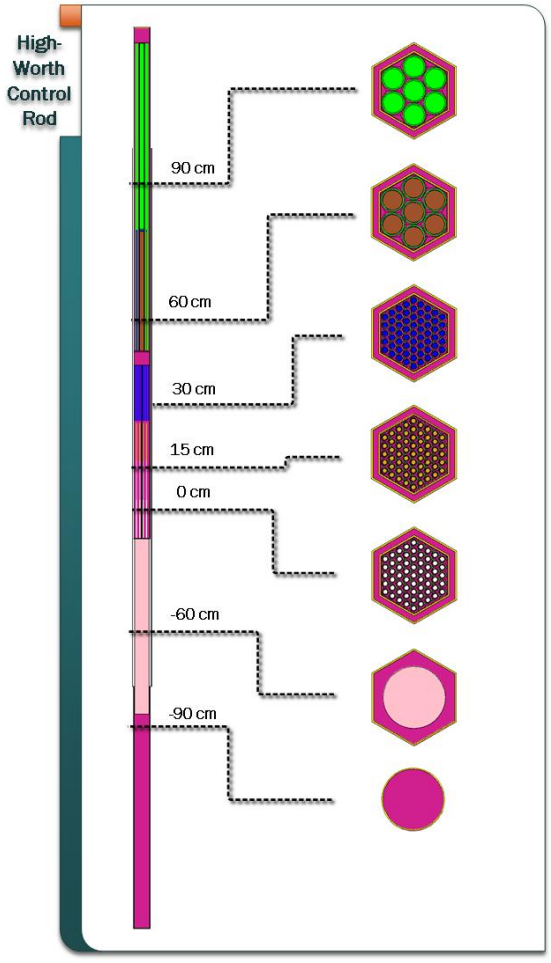

Figure 14. MCNP plot of a high worth control subassembly [26].

The control subassembly was nearly identical to the safety subassembly with only minor dimensional difference. The major difference was at full insertion into the core, the upper assembly would be above the reactor. At full withdrawal, the subassembly was flush with the core. Figure 15 shows how the different types of control subassemblies moved in the EBR-II core.

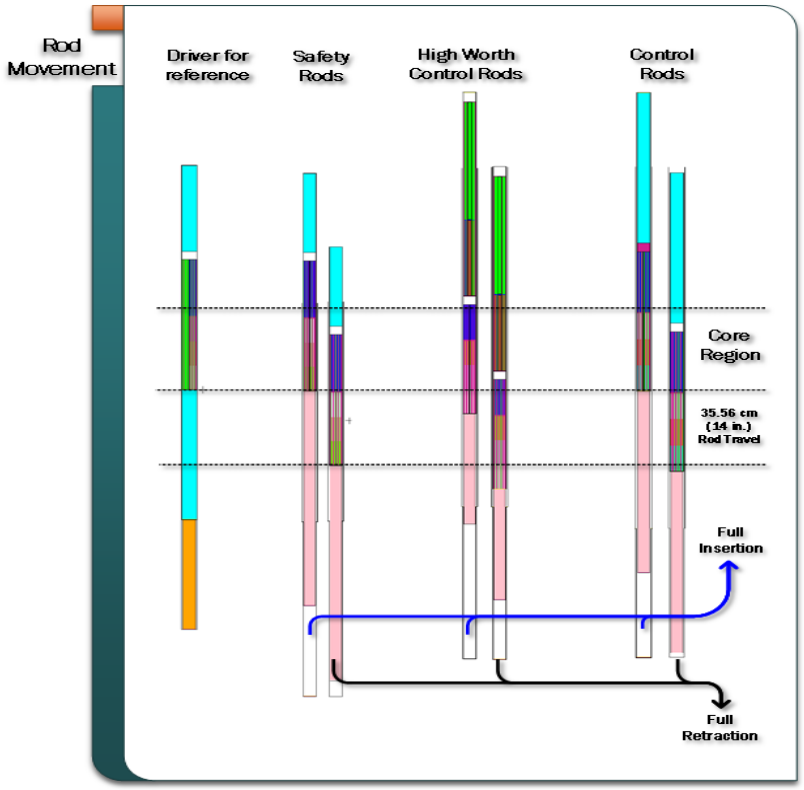

Figure 15. Control subassemblies movement [26].

The control subassembly had an inner hexagonal duct flat-to-flat inner diameter of 4.83 cm and an outer diameter of 4.90 cm. The inner hexagonal duct was comprised of three regions, an upper extension, core region, and lower adapter. The lower adapter was again modeled as a homogenized mixture of SS316 and sodium, with the same weight percent as the safety subassemblies, and had a length of 80.49 cm. The lower extension was 61.44 cm and had the same SS316 and sodium weight percent as the safety rod. The core region was 65.54 cm long and had 61 MKII fuel pins with a triangular pitch of 0.57 cm. The upper extension was 66.55 cm long and had the same SS316 and sodium weight percent as the safety rod. The outer hexagonal duct had a flat-to-flat inner diameter of 5.82 cm and outer diameter of 5.89 cm, along with a length of 159.82 cm. Figure 16 shows a control subassembly.

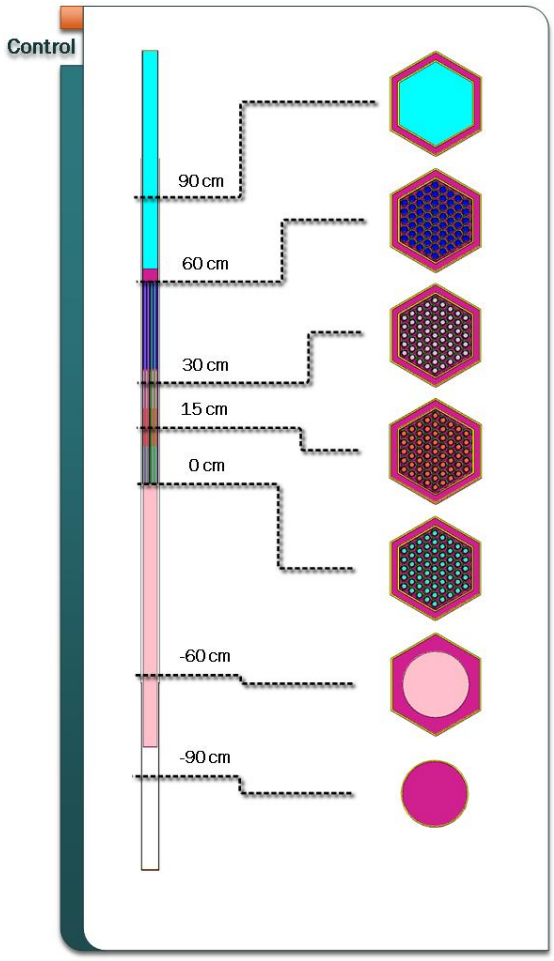

Figure 16. MCNP plot of the control subassembly [26].

The EBR-II core also contained seven experimental subassemblies during run 138B. Of the seven experimental subassemblies, three were nearly identical to the typical driver subassemblies with a slight alteration, and four had significant unique geometries not shared with any other type of subassembly.

The three subassemblies similar to typical driver subassemblies were C2776A, X412, and X320C. C2776A was designed like a driver subassembly, with the exception of xenon gas tags in the plenum of the fuel pins. X412 was identical to a driver subassembly with only minor material difference. X320C was similar to a stainless steel dummy pin, but was loaded with experimental materials for irradiation tests.

Experimental subassembly XX10 was similar to a safety subassembly due to it having a smaller inner hexagonal duct enclosed in the outer duct. The inner duct contained a lower adapter, fueled region, and upper extension. The core region contained 18 SS316 dummy pins and one hollow SS316 pin, each with a triangular pitch of 0.57 cm. All of this was contained in an inner hexagonal duct, with a flat-to-flat diameter of 4.826 cm and a wall thickness of 0.97 cm. The outer hexagonal duct had a flat-to-flat diameter of 5.82 cm, with a wall thickness of 0.10 cm.

Experimental subassembly XX09 was utilized as an instrumented subassembly, with a smaller hexagonal duct inside the larger hexagonal duct. The inner duct contained a lower adapter, fueled region, and upper extension. The core region contained 59 MKII fuel pins along with two hollow pins, which were arranged with a triangular pitch of 0.57 cm. The inner duct contained the lower adapter fueled region and upper extension, and had a flat-to-flat diameter of 4.83 cm, with a wall thickness of 0.97 cm. The outer duct had a flat-to-flat diameter of 5.82 cm with a wall thickness of 0.10 cm.

Experimental subassembly XY-16 was designed similar to a control subassembly except it was not moveable and it contained stainless steel dummy pins.

Experimental subassembly X402A was identical to a driver subassembly, with the exception of the central fuel pin being a hollow SS316 MKII pin filled with sodium instead of a fuel.

3.2.2 Detailed Description of Pin Types in MICKA

Fuel pins were placed inside drivers, half-worth drivers, safety, control, high-worth control, and experimental subassemblies. All of the fuel pins followed the general layout of a fuel slug,

followed by a sodium bond, and surrounded by a stainless steel cladding with a gas plenum above the fuel slugs. Run 138B was not a beginning of life core for EBR-II, this meant the fuel slugs, elements, and other components were swelled due to burnup from the length of time in the core. This causes many of the dimensions utilized in the MICKA model to reflect the swollen state. Due to the varying degree of burnup and swelling, the specific dimensions for the swollen state are not provided, but can be inferred from Appendix A. The dimensions presented in the following section provide the beginning of life measurements. The fuel slugs were 34.29 cm high with a diameter of 0.3302 cm. The fuel slugs were sodium bonded to the cladding material, and had additional sodium above the fuel to allow for greater heat conduction. The gas plenum was above the sodium bonded fuel and contained 75% helium with 25% argon, and was utilized to contain the gaseous fission products in the fuel pin. There were three types of fuel pins made: MKII, MKIIA, and MKIIS. The only difference between the fuel pins was the element height, and the sodium bond height above the fuel slugs. MKII had a fuel element length of 61.722 cm, with sodium filled 0.635 cm above the fuel. MKIIA had a fuel element length of 62.99 cm, with sodium filled 1.31 cm above the fuel. MKIIS had a fuel element length of 61.562 cm, with sodium filled 1.31 cm above the fuel. Each type of fuel was clad with stainless steel, typically SS316, but some experimental subassemblies used SS304, with a thickness of 0.0305 cm. Each pin also had a SS304 wire wrapped around it. The wire was 0.124 cm in diameter, and wrapped helically along the length of the fuel pin to prevent fuel pin claddings from interacting with each other and creating hot spots.

The stainless steel dummy fuel pins had the same dimensions as a typical MKII fuel pin, except the rod was solid SS316 or SS304. The MKII hollow pins in the experimental subassemblies

had a cladding width of 0.457 cm, and were filled with sodium. The dummy pins had a height of 145.28 cm with a diameter of 2.045 cm.

The B_4C poison pins were utilized in the high worth control subassemblies, slightly above the fueled region. These pins had a height of 91.676 cm, with a diameter of 1.588 cm, and a SS316 cladding thickness of 0.0889 cm. The poison slug region was 36.187 cm high and had a diameter of 1.4097 cm, with the remaining region being filled with 75% helium and 25% argon gas. The poison slugs had a height 35.552 cm with a diameter of 1.1 cm.

The outer blanket pins were similar in design to fueled pins. They contained a blanket slug, which was sodium bonded to the cladding with a gas plenum above. The pins had a height of 155.58 cm, with an outer diameter of 1.252 cm, and a SS304L wall thickness of 0.0457 cm. The blanket slug region was 142.75 cm in height with a diameter of 1.0998 cm. The blanket fuel slugs had a height of 139.7 cm with a diameter of 1.25 cm, and fit inside the blanket slug region.

3.2.3 Material Analysis for Fueled Subassemblies

The EBR-II core at the time of run 138B was composed of a variety of irradiated fuel, dependent on core location and length of time in the core. This meant the composition of subassemblies was extremely complex, due to fuel depleting at different rates. The data for the fuel and material compositions was obtained from ANL, document ANL-ARC-228 [25]. These data contained a depletion analysis which lumped fission products together, except for lanthanum-139 and neodymium-148. For a detailed analysis, the individual fission products were needed to create an adequate model for use in MCNP. This fuel depletion analysis was performed by Jordan Sheppard utilizing SCALE6.1 with the Transport Rigor Implemented

with Time-dependent Operation and Neutronic depletion (TRITON) control module [27]. The depletion analysis was done with TRITON on a single fuel assembly, both a driver and a blanket, with radial mirror reflection, to simulate subassemblies on all sides. This approach was taken to make the process quicker and more efficient, rather than trying to perform a full depletion analysis on the entire core. Previous existing reactor information provided a burnup amount, and the specific burnup time was selected to match the ANL report results for uranium-235, plutonium-239, lanthanum-139, and neodymium-148.

A typical fuel pin contained approximately 47 g of uranium-235 for each of the 91 fuel pins in a subassembly. This meant in a driver subassembly, there was approximately 4.3 kg of uranium-235. There were approximately 8,260 fuel pins in the central core region, which gives a total uranium-235 content for the core of approximately 388 kg.

3.3 Homogenization of Subassemblies

3.3.1 Methodology of Homogenization

Due to the complexities and amount of detail of the EBR-II core in the MICKA model, it was found additional simplifications would be needed for the ease of future use. These simplifications came in multiple steps. The first step was the removal of the lower cylinders, followed by homogenizing the blanket region, reflector region, dummy subassemblies, half-worth driver subassemblies, and driver subassemblies. This process was chosen to examine the effects of homogenization during each step, to determine if appropriate bias factors were needed, along with their applicability and limitations for the benchmark project [7].

The homogenization process followed two basic questions; the ease of homogenization, and the assumed severity to the multiplication factor and the control rod worth. The first choice for

homogenization was the removal of the smeared lower cylinder. This was chosen for its ease of material and geometric simplification, and due to its distance away from the core region. This process was done in two separate phases to determine individual and integral effects to k_{eff} when removing the lower cylinder. Once this process was complete, and results were obtained, the smeared lower cylinders were placed back into the model and the homogenization process for the remainder of the model took place. This process was also done first to determine the effect on k_{eff}, given the lower cylinder removal. During each step of the homogenization process it was important to know the effect due to the removal of the lower cylinder.

Each section of the reactor core was taken from the detailed MICKA model, and each subassembly was homogenized. During this homogenization process, different sections of the subassembly were accounted for and homogenized accordingly. For example, the blanket region would turn from individual subassemblies into one hexagonal shaped homogenization of blanket pins and sodium coolant. This method was slightly changed in the core central core region. For the dummy, half-worth driver, and driver subassemblies, the outer hexagonal duct was left in place and only material inside the duct was homogenized. This was done to align with methods found in Duderstat and Hamilton, and maintain consistency between the MCNP and SCALE models. Once each section was completed, and the results were obtained, it was returned to the detailed model for the next section of homogenization. Once each section of the reactor core was homogenized and the results were obtained, the homogenized pieces were combined separately to determine the integral effects of homogenizing the core. There were two main sections of the EBR-II core not homogenized, the experimental subassemblies and the control/safety/and high worth control rods. It was determined the experimental subassemblies were not characterized well enough to warrant investigation into any

homogenization effects. Due to the extreme complexity in the creation of the control rods in MICKA, homogenizing the control rods was not feasible. The main complexity was the movement of the control rods. MICKA built the control rod subassemblies based on a user defined input. This meant each section of the control rod had to be moved a specified distance. Due to this, trying to remove specific sections of the control rods for the homogenization process without interfering with the codes ability to move was problematic. Along with this, the control rods were determined to have a similar effect to homogenizing a driver subassembly due to the fact they were fueled subassemblies with smaller fuel loading.

During the homogenization process, each homogenized section was run twice. Once with the control rods fully withdrawn (the subcritical configuration) and once with the control rods at their critical configuration [6]. This would allow for a comparison in the control rod worth and k_{eff} for both the critical and subcritical configuration. Figure 17 shows a cross section of the MICKA core region with the control rods at the critical configuration, while Figure 18 shows a cross section of the MICKA core region with the control rods at the subcritical configuration. Both figures show a cross-section of the core at the bottom of the core region to show the control rod movement. Table 3 shows the height of the control rods at their critical configuration. Each control subassembly was 0.0 cm inserted for the subcritical configuration.

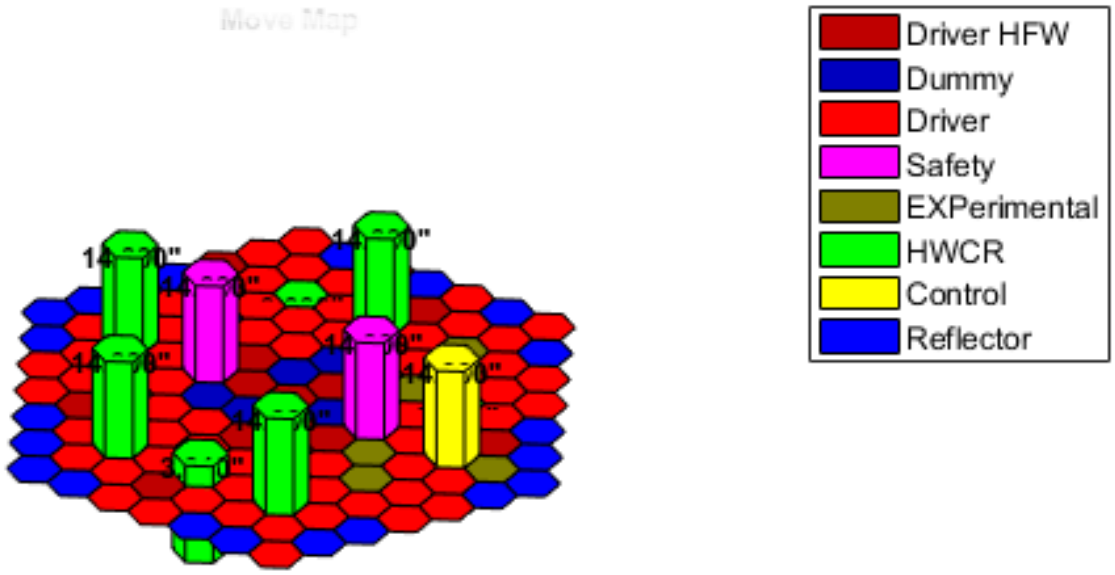

Figure 17. Control rods in the critical configuration.

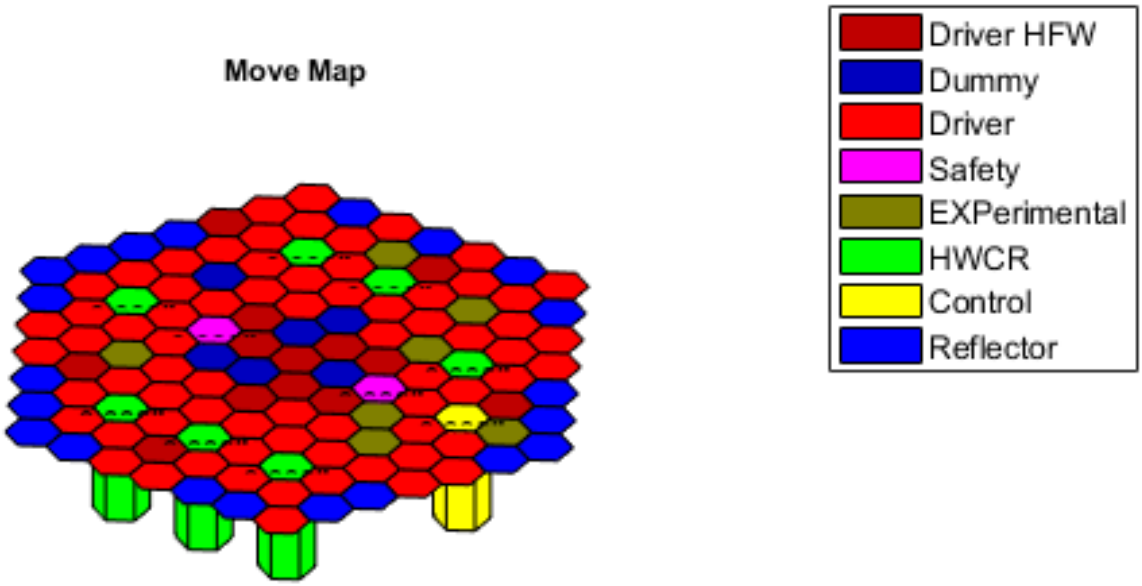

Figure 18. Control rods in the subcritical configuration.

Table 3. Control Rod Height for Critical Configuration

Control Subassembly	Critical (in/cm)
03D01 Safety	14 / 35.56
03A01 Safety	14 / 35.56
05C03 HWCR	0 / 0
05D01 Control	14 / 35.56
05E01 HWCR	14 / 35.56
05E03 HWCR	3.01 / 7.6454
05F01 HWCR	14 / 35.56
05A01 HWCR	14 / 35.56
05B01 HWCR	0 / 0
05B03 HWCR	14 / 35.56

3.3.2 Blanket Region

After the removal of the lower cylinders, the first step of the homogenization process involved homogenizing the individual subassemblies in the blanket region. This process left out the lower adapter and focused on the fuel, sodium bonded region, plenum, fuel cladding, sodium coolant, and hexagonal duct. The first step was to determine the appropriate volumes for each homogenized portion. The engineering drawings were utilized to find dimensions for each contributing volume, and then yield a volume fraction which could be used to homogenize the section. The total volume was found to be 4805.56 cm^3. The volume fraction results for the blanket homogenization phase are found in Table 4.

Table 4. Volume Fractions for Blanket Subassemblies

	Individual Volume (cm^3)	Total Volume (cm^3)	Volume Fraction (%)
Fuel Pin	132.72	2521.64	52.47
Sodium Bonding	18.35	348.66	7.26
Plenum	13.48	256.08	5.33
Fuel Cladding	27.05	513.99	10.70
Sodium Coolant	832.53	832.53	17.32
Hex duct	332.67	332.67	6.92

Using the volume fractions, the homogenization process involved taking the material composition of each component, multiplying it by the volume fraction, and then summing up

the materials. An individual blanket fuel pin, for example, required multiple steps. The blanket fuel pin was divided into three sections; each of which were unique in their material cards due to burnup. Each section of the 19 pins were summed, and then multiplied by 17.49%, which is the volume fraction for the section of fuel pins. This yields the material contribution due to each section of the fuel pin. The material from the sodium bond was multiplied by 7.26%, the volume fraction for all of the fuel pins sodium bond, to find the material contribution from the sodium bond. The plenum material was multiplied by 5.33%, to find its material contribution. Finally, the fuel cladding was found by multiplying its material contributions by 10.70%. The sodium coolant and hexagonal duct materials contributions were multiplied by 17.32% and 6.92% respectively. All the isotopes were used to create a new material, any isotopes that appeared multiple times from different sections were summed. The new blanket was then constructed utilizing the new material card and replacing the individual components with one hexagonal homogenized cell. This cell has the dimensions of the hexagonal duct, with a diameter of 5.82 cm, and a height of 155.5 cm.

3.4 Selection and Homogenization of a Driver Subassembly in SCALE

An individual driver subassembly was chosen to be analyzed in SCALE to perform an in-depth sensitivity and uncertainty analysis. Due to the large degree of spatial variation in the EBR-II core, it was important to find a subassembly which best minimized potential discontinuities in the core. Subassembly 04E01 was surrounded by driver subassemblies which all had similar power densities, and was chosen for examination [27]. The SCALE input file was originally created by Jordan Sheppard for a masters' project, and adjusted by Emerald Ryan for

sensitivity analysis [28]. Once this file was obtained, it was changed from a multi-group cross-section set to a continuous energy group for analysis.

The driver subassembly was modeled in SCALE in accordance to the design described in section 3.2.1. The only difference was removal of the lower smeared cylinder for the SCALE model for simplification. Figure 19 shows the plan and elevation view of the fuel region in the SCALE heterogeneous model.

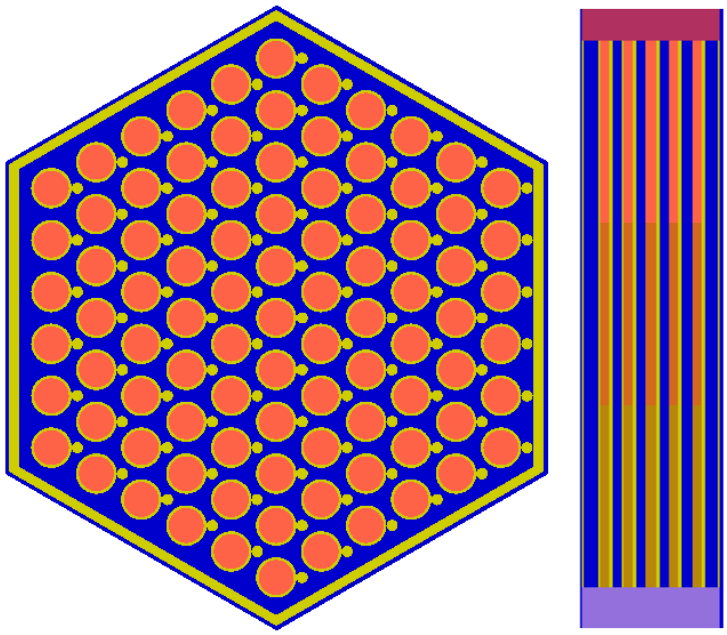

Figure 19. Plan and elevation view of fuel region in SCALE heterogeneous model.

To homogenize the fueled region, the volumes of each individual component were calculated and then used for the volumetric fraction when homogenizing. The outer hex duct was not homogenized into the fueled region, to prevent an artificially high amount of stainless steel in the homogenized material. This is practiced in boiling water assemblies when homogenization is taking place, and was adopted for this model [11]. Table 5 shows the volume, and the volumetric fraction for each component in the fueled section.

Table 5. Volume Fraction for a Driver Subassembly

	Individual Volume (cm^3)	Total Volume (cm^3)	Volume Fraction (%)
Lower Fuel Section	1.39	126.75	13.52
Middle Fuel Section	1.39	126.75	13.52
Upper Fuel Section	1.40	127.68	13.62
Fuel Cladding	1.44	131.30	14.00
Wire Wrap	0.45	40.58	4.33
Sodium	384.57	384.57	41.02

The volume fractions from Table 5 were applied to the atom densities for each respective material (See Appendix B) and each nuclide; the nuclides were then used to create one material card which was utilized by SCALE. Figure 20 shows the plan and elevation view of the fuel region in the homogeneous model, where the change from pink to maroon and purple signify the change from fueled region to upper and lower extension.

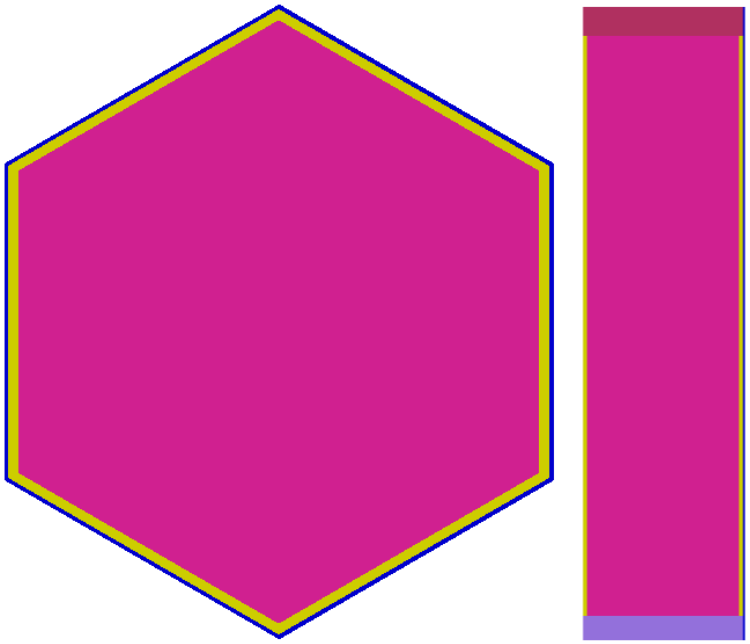

Figure 20. Plan and elevation view of fuel region in SCALE homogeneous model.

4.0 Simplified Simulation Model

4.1 MCNP Model and Development

The Monte Carlo simulation for the homogenization process of the EBR-II core utilized MCNP6 version 1.0.0 [8]. The calculations were performed on the high-performance computing cluster, PLEXI, at Idaho State University [29]. MCNP6 utilized the parallel processing capabilities, inherently built in, and spread the simulation across 24 separate nodes. MCNP6 version 1.1.0 was released at this time, but was not installed on PLEXI. Due to this fact, there is a small shift in the k_{eff} between the two versions. From MCNP6 version 1.1.0, the detailed k_{eff} value was found to be 1.00601 ± 0.00006, while on MCNP 6 version 1.0.0, k_{eff} was found to be 1.00614 ± 0.00006. Despite this shift, the ability to rapidly perform the MCNP calculations outweighed the slight shift in k_{eff} and each run was compared to the version 1.0.0 detailed model. The data obtained from version 1.0.0 gave a relative difference, not an absolute difference. To run MCNP6 an input file is built using three input sections, which describe the cells, surfaces, and data for the problem.

The cell cards describe three dimensional geometries utilizing the surfaces from the surface section, and combines them with Boolean logic to make combinatorial geometry [30]. The surfaces can come either as macro bodies (such as cylinders and right hexagonal prisms) or as plane surfaces (such as an x-plane or infinite cylinder). Each cell card follows a similar format, with the first number being its unique identifier, followed by the material number, which is from the data cards. This is followed by the density of the material, where a negative represents mass density (in g/cm^3) and a positive value is an atom density. This is followed by a combination of surface cards, using Boolean logic, where a negative indicates inside the surface, and a positive indicates outside the surface. There are also a few optional sections

which can indicate a universe or lattice, depending on where in the system the geometry is located. Finally, the importance of the particle must be specified, where an importance of zero indicates the particle will no longer be tracked.

The cell cards created by MICKA are approximately 20,000 lines long (including comments) and comprises the entire EBR-II core. Each specific geometry is numbered according to the specific subassembly in the core, and each subassembly has its own universe number attached to it. For example, the blanket subassembly 16C10 has each geometric cell follow the numbering between 7832-7945, depending on when the cell was made in MICKA. The universe number is designated with 700xxx, where the xxx depends on the section of the subassembly. Any subassembly that has separated pins is placed into a hexagonal lattice, and the subassembly itself is placed into a larger hexagonal lattice which encompasses the entire core.

The surface cards created by MICKA are approximately 10,000 lines long (including comments), and writes the surfaces for every component in the EBR-II core. In MCNP, the surface cards are made up of surfaces, or macro bodies, which are utilized to create three dimensional geometries. The surface entries start with an identifying number, followed by the shape or plane represented. For example, a right circular cylinder is designated with RCC, and a plane in the Z-direction is designated with PZ. The macro bodies and surfaces are then followed by the particular number of entries needed to create the shape or plane. For the MICKA input file, each subassembly starts with the outer hex duct and is designated with a three-digit number that increases as the subassembly grows from the core center. The rest of surface identifying values range in near linear order, where there are between five and sixteen surfaces per subassembly.

The data cards created by MICKA are approximately 100,000 lines long (including comments), and are mainly comprised of materials. In MCNP the data card is made of materials, operation parameters, and tallies used to describe the problem. The material card begins with a user assigned value, and is followed by the isotopes in the media, which are given by their identification or ZAID number. For example, uranium-238 would be designated as 92238, where 92 is the atomic number followed by 238, which is the isotope. Attached to the ZAID number is a .xxc which denotes which cross-section set is to be used. After each specified isotope, either the atomic fraction or the weight fraction is given, where the atomic fraction is a positive value, and the weight fraction is denoted by a negative value. The MICKA materials are designated an assigned value based on the MICKA number of the subassembly. For example, subassembly 16C10 has a MICKA number of 641, which correlates to a material assigned value 641xxxx.

The MCNP data card also contains operation parameters and tallies. These parameters encompass where to include the starting source, how many generations to run, how many particles to run, and how many generations to skip. Along with this, it allows the user to control what types of data to print. The tallies allow the user to determine values such as flux and fluence. For the MICKA input, it was determined that 1010 generations, each with 100,000 neutrons while skipping 10 generations would provide sufficient statistical data. The neutron source for the first generation had one point in each of the driver subassemblies. Along with this, there were parameters to help reduce the size of the output file to make it manageable to view. A sample MCNP input file can be seen in Appendix D.

4.2 MICKA to MCNP

Due to the sheer number of subassemblies and the detail attributed to each subassembly, it was determined MICKA would be used to create an individual input file for each homogenization step. To allow for this, MICKA had to be altered in two main ways. The first, was the generation of new MATLAB functions to create a homogenized subassembly [31]. The second was integrating the new MATLAB functions into the framework of MICKA.

The generation of the new MATLAB functions involved creating new functions. These functions brought data for a specified type of subassembly, manipulated these data, and then formed new data for the MCNP input file. The first step of this process was to take in the dimensions, materials, and origins for the original subassembly type. For example, a blanket element would have the dimensions, materials, and origin for each blanket subassembly. The dimension, material and origin information would then get passed to multiple sub-functions. These sub-functions grew out of a necessity for an ease in code development and streamlining the process. For a list of lessons learned while programming see Appendix C. These sub-functions calculated the volumes and volume percent for each component of the subassembly for the homogenization process. Along with this, they converted material data in both weight percent and atom percent to atom density, which is then used to create one material for the entire homogenized region. Finally, data for the material composition and density was passed to the main subassembly creation function, which would print out the new material being used, along with cell and surface cards. This information is then fed back into the main program of MICKA to write the MCNP input file. Figure 21 shows the original algorithm for MICKA building the EBR-II core. Figure 22 shows the modifications that went into building the homogenized subassemblies in MICKA for the EBR-II core.

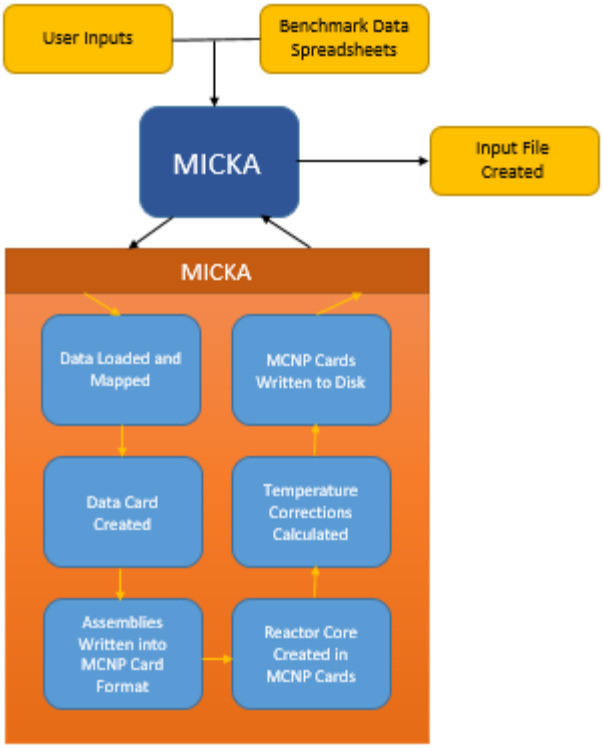

Figure 21. MICKA flow chart.

Figure 22. MICKA flow chart with homogenization function additions.

4.3 SCALE Model and Development

The sensitivity and uncertainty analysis for the EBR-II driver subassembly was performed using SCALE 6.2.1 [32]. KENO VI was used for the Monte Carlo calculations, while TSUNAMI-3D was used for the sensitivity and uncertainty analysis. The calculations were performed with a Windows 10 operating system, operating with eight processors. The processors were Intel Core i7 CPUs operating at 2.50 Ghz.

KENO VI follows a similar file format to MCNP. The materials are input first, and assigned a value to be called upon when referencing them. An isotope, element, or combination of the

two can be mixed together to create a material. Following each element, an atom density (or a density with a corresponding temperature) is listed. This format can be varied if introducing a material in terms of weight percent, which KENO converts to atomic density for calculations. For the heterogeneous model, there were sixteen materials, of which six were sodium and SS316. The sodium had multiple materials created to examine the difference in sodium sensitivity between the sodium bond, the sodium in the hex duct, and the sodium around the hex duct. Similarly, SS316 had different materials to examine the sensitivities between the cladding, wire wrap, and hex duct. The materials representing the fueled sections and the smeared sodium-SS316 upper and lower sections were input as a weight percent. Sodium was entered without impurities as a natural element. SS316's isotopic content and atomic density were the SCALE manual's built-in material [18]. The homogeneous model utilized eight materials. The smeared upper and lower extensions were input as weight fractions. The fueled section was input as an atomic density, with an average temperature. The SS316 and sodium remained the same as the heterogeneous model.

The geometry building tools in KENO VI are also similar to MCNP. Macro bodies were used to create objects like cylinders and right hexagonal prisms. KENO VI defines the macro bodies, which are then filled with a material by media cards. Media cards designate materials based on being inside or outside a macro body. To create the geometry of the heterogeneous EBR-II driver subassembly in SCALE, a series of five cylinders were combined to create the multiple fuel pin sections, fuel cladding, and wire wrap. These pins were then placed into a right hexagonal lattice of sodium, which were subsequently placed into the 91 fuel pin array, surrounding the fueled section as the stainless steel hexagonal duct. For the upper and lower extension, a right hexagonal prism the size of the hexagonal duct was used. This was all

surrounded by a thin right hexagonal prism of sodium. The homogeneous model utilized a right hexagonal prism for the fueled region, which had a material smear of fuel, cladding, wire wraps, and sodium. The outer hexagonal duct, upper and lower extension, and sodium layer remained the same as the heterogeneous model. A sample SCALE input file can be seen in Appendix E.

KENO VI was utilized in SCALE to run through the Monte Carlo statistical sampling. The heterogeneous model ran with 6500 generations, each with 5000 particles. During the run, the first 500 generations were skipped to allow for the fission source to converge before beginning the averaging techniques. The homogeneous model ran 6500 generations, each with 5000 particles and 500 generations skipped. This allowed for a total of 30,000,000 tracked particles for the heterogeneous and homogeneous models. For the heterogeneous system, the run time was significantly longer for an individual generation, thus the overall time was greatly increased. To run the sensitivity analysis, TSUNAMI-3D used continuous energy cross-section sets with the IFP method, where five latent generations were skipped.

4.3.1 Direct Perturbation

To ensure TSUNAMI is performing the sensitivity analysis correctly, it is strongly suggested a direct perturbation is performed [23]. This suggestion stems from the fact that the sensitivity parameters are strongly dependent on the user inputs. The inputs include the latent generations in the IFP process, and the number of particles run. A direct perturbation was performed using the information from section 2.2. The general guideline to ensure the direct perturbation yields an accurate response is to have the Δk between the original and perturbed models (around ±0.5%). Values higher than this may not be in the linear region of first-order perturbation

analysis [33]. Smaller values may not show a significant change, or the change may be within the uncertainty of the original model [33]. Once the results are obtained, a difference between the direct perturbation and TSUNAMI should be within 5% and/or less than 0.01 in absolute sensitivity to obtain quality results [24].

The first step in the direct perturbation was to obtain the results of the sensitivity parameter for the original model. Next, the uranium-235 atom density was perturbed by ± 2%. For the homogeneous model, there was only one value for uranium-235 in the homogenized smear, and it was perturbed by 2%. For the heterogeneous model, there were three sections of fuel elements, and all three sections had their uranium-235 densities perturbed by 2%. The simulation was re-run to determine a new k_{eff} value for both the positive and negative perturbation. Once data was collected, the different k_{eff} values and the atom densities were run through Equation 5 from section 2.2 to obtain the direct perturbation sensitivity coefficient. The sensitivity coefficient was then compared to the sensitivity value from the TSUNAMI-3D results to determine if the user defined input parameters are valid. To ensure proper analysis, and to examine the effects of incorrect atom density perturbations, the atom density was also perturbed by 1%, 0.5%, and 0.25%.

5.0 Simulation Results

5.1 Removal of Lower Cylinder

The first phase in the homogenization process was to examine the impact of removing the lower cylinder from each of the subassemblies. This process was done in two phases, each with five steps. The first phase homogenized individual subassembly type, and the second phase followed an integral homogenization process. The five steps utilized in each phase are; step 1:

blanket subassemblies, step 2: reflector region, step 3: dummy subassemblies, step 4: half-worth driver subassemblies, and step 5: driver subassemblies. To determine the effects, each step was run twice, with the control rods fully inserted (subcritical) and at the critical rod height for run 138B [6]. Table 6 shows the k_{eff}, uncertainty, and percent difference for each step of the process, with the detailed run for reference.

Table 6. Criticality for the Individual Lower Cylinder Removal

	k_{eff}	Uncertainty	k_{eff} Difference (pcm)
Detailed Critical	1.00614	0.00006	
Detailed Subcritical	0.97699	0.00006	
Step 1 Critical	1.00596	0.00006	-1.789
Step 1 Subcritical	0.97700	0.00006	1.024
Step 2 Critical	1.00605	0.00007	-0.895
Step 2 Subcritical	0.97719	0.00006	2.047
Step 3 Critical	1.00607	0.00006	-0.696
Step 3 Subcritical	0.97709	0.00006	1.024
Step 4 Critical	1.00302	0.00006	-1.192
Step 4 Subcritical	0.97706	0.00006	0.716
Step 5 Critical	1.00604	0.00006	-0.993
Step 5 Subcritical	0.97714	0.00006	1.535

Each of the steps maintained a k_{eff} within five per cent mille (pcm) of the detailed model. This initial result seemed promising for the removal of the lower cylinder in the homogenized model. To further determine the lower cylinder removals viability, the control rod worth was examined when the lower cylinders were removed. Table 7 shows the control rod worth, the percent difference and the corresponding dollar value for each step.

Table 7. Control Rod Worth for the Individual Lower Cylinder Removal

	Control Rod Worth ($)	Control Rod Worth Difference (%)	Control Rod Worth Difference ($)
Detailed	4.242		
Step 1	4.215	-0.6518	-0.028
Step 2	4.200	-0.9949	-0.042
Step 3	4.218	-0.5832	-0.025
Step 4	4.215	-0.6518	-0.028
Step 5	4.206	-0.8576	-0.036

The most dramatic changes for the individual lower cylinder removal occurred within the second step, when the reflector subassemblies had the lower cylinder removed. During the final step, the change in control rod worth was within five cents of the detailed model, and caused a -3.6 ¢ change in the control rod worth. Overall, the individual lower cylinder removal provided confidence in the next step of the lower cylinder removal process, which was the integral removal of the lower cylinder.

The integral removal of the lower cylinder was performed in the same steps as the individual removal process. This meant step 1 was the removal of the blanket lower cylinder, step 2 was the removal of the blanket and reflector lower cylinder, and so forth. Both k_{eff} and the control rod worth was examined for the integral removal, and the results can be seen in Table 8 and Table 9.

Table 8 Criticality for the Integral Lower Cylinder Removal

	k_{eff}	Uncertainty	k_{eff} difference (pcm)
Detailed Critical	1.00614	0.00006	
Detailed Subcritical	0.97699	0.00006	
Step 1 Critical	1.00596	0.00006	-1.789
Step 1 Subcritical	0.97700	0.00006	1.024
Step 2 Critical	1.00599	0.00006	-1.093
Step 2 Subcritical	0.97706	0.00006	1.228
Step 3 Critical	1.00603	0.00007	-1.093
Step 3 Subcritical	0.97711	0.00006	1.223
Step 4 Critical	1.00603	0.00007	-1.093
Step 4 Subcritical	0.97723	0.00006	2.456
Step 5 Critical	1.00594	0.00006	-1.988
Step 5 Subcritical	0.97695	0.00006	-0.409

Table 9 Control Rod Worth for the Integral Lower Cylinder Removal

	Control Rod Worth ($)	Control Rod Worth Difference (%)	Control Rod Worth Difference ($)
Detailed	4.243		
Step 1	4.215	-0.6518	-0.028
Step 2	4.210	-0.7547	-0.032
Step 3	4.209	-0.7890	-0.033
Step 4	4.192	-1.201	-0.051
Step 5	4.219	-0.5489	-0.023

The most dramatic changes for the integral lower cylinder removal occurred within the fourth step, when the blanket, reflector, dummy, and half-worth subassemblies had the lower cylinder removed. During the final step, the change in control rod worth was within five cents of the detailed model, and caused a -2.3 ¢ change in the control rod worth. Overall, the integral lower cylinder removal provided confidence that the removal of the lower cylinder would not have a detrimental impact on k_{eff} throughout the remainder of the homogenization process.

5.2 Homogenization of the EBR-II Core

The second phase in the homogenization process was to homogenize the remainder of the EBR-II core. This was done in multiple steps, each with two simulated models. Each step was

run with the control rods in two separate configurations, one with the control rods critical, and one with the control rods fully removed [6]. The homogenization process followed section 3.3 and were as follows; Step 1: blanket region, Step 2: reflector region, Step 3: dummy subassemblies, Step 4: half-worth subassemblies, Step 5: driver subassemblies. Table 10 through Table 13 provide the data from each step of the homogenization process for both k_{eff} and the control rod worth.

Table 10. Criticality for EBR-II Homogenized Core with Individual Steps

	k_{eff}	Uncertainty	k_{eff} Difference (pcm)
Detailed Critical	1.00614	0.00006	
Detailed Subcritical	0.97699	0.00006	
Step 1 Critical	1.00047	0.00006	-56.35
Step 1 Subcritical	0.97135	0.00007	-57.73
Step 2 Critical	0.99401	0.00006	-120.6
Step 2 Subcritical	0.96563	0.00006	-116.3
Step 3 Critical	1.01017	0.00006	40.05
Step 3 Subcritical	0.98124	0.00006	43.50
Step 4 Critical	0.99880	0.00006	-72.95
Step 4 Subcritical	0.96945	0.00006	-77.18
Step 5 Critical	0.90986	0.00006	-956.9
Step 5 Subcritical	0.87651	0.00006	-1028

Table 11. Criticality for EBR-II Homogenized Core with Integral Steps

	k_{eff}	Uncertainty	k_{eff} Difference (pcm)
Detailed Critical	1.00614	0.00006	
Detailed Subcritical	0.97699	0.00006	
Step 1 Critical	1.00047	0.00006	-56.35
Step 1 Subcritical	0.97699	0.00006	-57.73
Step 2 Critical	0.99263	0.00007	-173.6
Step 2 Subcritical	0.95997	0.00006	-174.2
Step 3 Critical	0.99263	0.00007	-134.3
Step 3 Subcritical	0.96437	0.00006	-129.2
Step 4 Critical	0.98056	0.00007	-209.5
Step 4 Subcritical	0.95621	0.00006	-212.7
Step 5 Critical	0.88603	0.00006	-1193
Step 5 Subcritical	0.85279	0.00006	-1271

Table 12. Control Rod Worth for EBR-II Homogenized Core with Individual Steps

	Control Rod Worth ($)	Control Rod Worth Difference (%)	Control Rod Worth Difference ($)
Detailed	4.242		
Step 1	4.238	-0.1029	-0.004
Step 2	4.130	-2.642	-0.112
Step 3	4.210	-0.7547	-0.0320
Step 4	4.272	0.6861	0.0291
Step 5	4.854	14.41	0.611

Table 13. Control Rod Worth for EBR-II Homogenized Core with Combined Steps

	Control Rod Worth ($)	Control Rod Worth Difference (%)	Control Rod Worth Difference ($)
Detailed	4.242		
Step 1	4.238	-0.1029	-0.004
Step 2	4.130	-1.516	-0.064
Step 3	4.113	-3.053	-0.130
Step 4	4.199	-1.029	0.029
Step 5	4.838	14.03	0.595

As expected, the most dramatic impact on criticality was the homogenization of the driver subassemblies. This impact strongly correlates with the fact that the majority of neutrons are born and absorbed in the central core region, and thus the central core region has the most impact on k_{eff}. The drop in k_{eff} due to homogenization fits with the theory from section 2.2. To examine the impact on k_{eff} further, there are two important values to examine to fit theory with reality; the flux weighted energy and the average mean free path.

The MCNP output file provides the flux weighted energy for individual cells within the EBR-II core, which can be used to determine the homogenization effects on the average neutron energy. To be able to compare the heterogeneous and homogeneous results, the data for the heterogeneous model had to be volume averaged over all the cells which made up the subassembly. This volume averaging process was identical to the process from section 3.3.1. Once the volume average values for the flux weighted energy were obtained, the values were plotted in Figure 23 to determine general trends in the data. The subassemblies chosen for

comparison were subassemblies in a line directly from the center of the core and are described in Table 14.

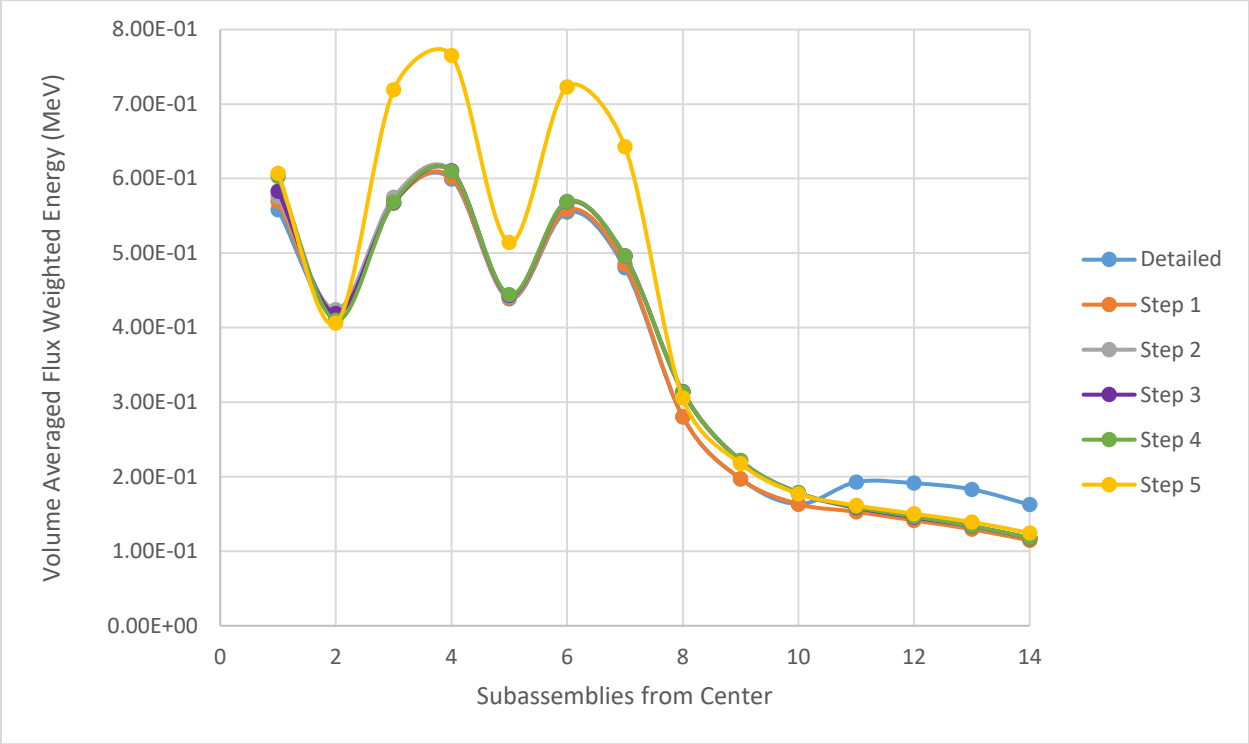

Figure 23.Volume averaged flux weighted energy vs. distance from EBR-II center.

Table 14. Subassembly Description for Flux Weighted Energy and Mean Free Path

Subassembly Number	Subassembly Type
01A01	Hal-Worth Driver
02B01	Dummy
03B01	Driver
04B01	Driver
05B01	High Worth Control Rod
06B01	Driver
07B01	Driver
08B01	Reflector
09B01	Reflector
10B01	Reflector
11B01	Blanket
12B01	Blanket
13B01	Blanket
14B01	Blanket

From Figure 23, there are multiple conclusions that can be drawn about the homogenization effect on the average energy. Throughout the homogenization process, the effect on the average energy was minimal until the driver subassemblies were homogenized. The final step in the homogenization process increased the average neutron energy by approximately 15% for each driver subassembly. The increase in average energy is due to a decrease in thermalization from sodium. Although the sodium makes up over 50% of the driver volume, the density is greatly reduced in the homogenized model due to its low density in comparison to the cladding and the fuel, which reduces its relative effectiveness in moderating neutrons. It is important to note the drop in the average energy for 05B01. This subassembly is a high worth control rod subassembly, and was not homogenized which causes a large shift in the average energy which aligns with the detailed model. The other important information to gain from Figure 23 is the average energy in the core region. It is noted that the average energy throughout the core for the detailed model, and for the homogenized model steps 1-4, is around 0.5 MeV. Alternately, for the fully homogenized model, the average energy is around 0.6 MeV, about 15% higher. This shift in the average energy can again be best described by the lack of thermalization due

to sodium. This effect was well demonstrated in CP-1, described in section 2.2. For both CP-1 and EBR-II, as the average energy in the system increases due to homogenization, which causes k_{eff} to decrease due to the decrease in the fission cross section for uranium-235 relative to the absorption cross sections of the other materials. The decrease in the fission cross section for uranium-235 implies that to stay critical, the mass of uranium-235 must increase.

Along with the average energy of the core region, it important to determine the effect of homogenization of the averaged mean free path through the core. To be able to compare the detailed and homogenized models, the volume average approach was used in the same way as the flux weighted average energy. Along with this, the same subassemblies in Table 14 were compared, and the results can be seen in Figure 24.

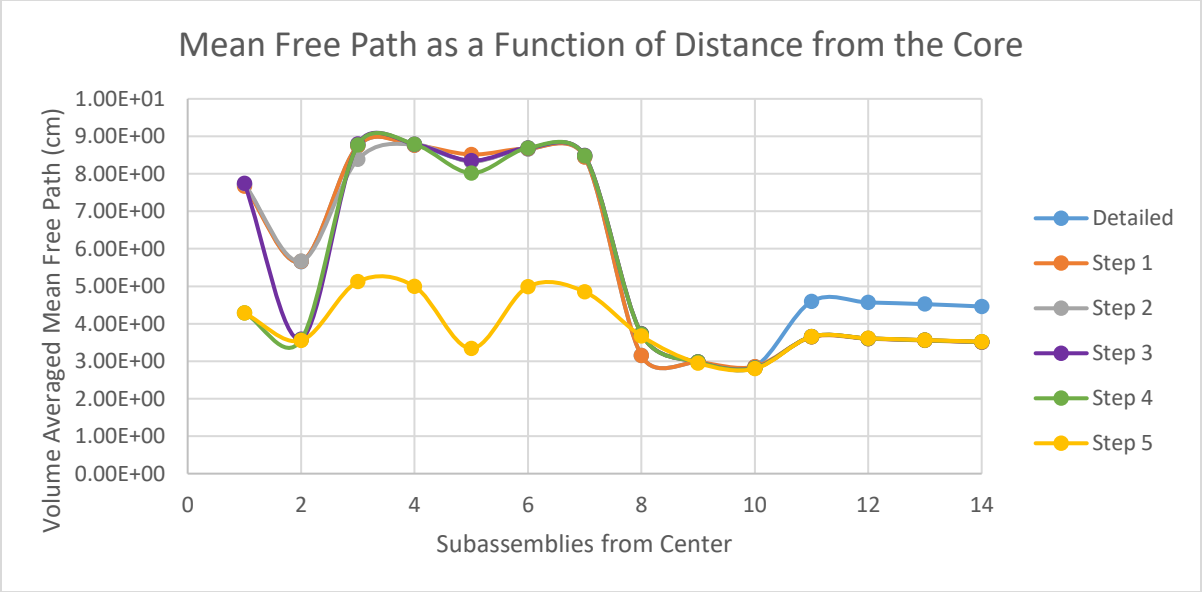

Figure 24. Average mean free path vs. distance from EBR-II center.

Figure 24 provides information on how neutrons travel and interact within the EBR-II core. The first important aspect is whenever homogenization occurred, the volume averaged mean free path decreased. Similar to the flux weighted energy, the homogenization of the driver

subassemblies shows the most pronounced effect and causes a decrease in the mean free path of nearly 60%. This is largely due to the sodium content being homogenized with denser materials, which increases the atom density, and decreases a neutron's ability to traverse a subassembly without an interaction. The outlying factor is the fifth subassembly, where there is a large spike in the mean free path due to this subassembly being a high worth control rod and not being homogenized, thus it retained its detailed value. Despite the drop in mean free path for the homogenized model, it is important to note the overall shape of the mean free path throughout the core remains similar to the heterogeneous model. This correlates strongly with the results from the volume averaged flux weight average energy and the SCALE model to help reinforce the fact that the homogenization effects the magnitude but not the underlying physics occurring within the EBR-II core.

5.3 Direct Perturbations

The direct perturbation was performed for both the heterogeneous and the homogeneous models to ensure TSUNAMI was calculating the uncertainties correctly with the given user inputs. To obtain an accurate result for the homogeneous model, a Δk of $\pm 0.5\%$ (~0.00907) was desired. As mentioned in section 4.3.1, the total uranium-235 atom density was perturbed

by 2%, 1%, 0.5% and 0.25%. Table 15 shows the sensitivity values for the multiple first order perturbations.

Table 15. Sensitivity Parameters for Direct Perturbations in the Homogenous System

Atom Density Perturbations	Average Δk	Sensitivity Parameter	Difference in Sensitivity Parameter (%)
TSUNAMI		0.17404	
2%	0.00620	0.17084	-1.87
1%	0.00309	0.17001	2.31
0.5%	0.00162	0.17745	-1.96
0.25%	0.00085	0.18737	-7.66

The desired response of 0.00907 was most closely achieved by the 2% perturbation to the uranium-235 atom density. Table 15 presents the fact that the smaller the atom density perturbation, the more volatile the sensitivity parameter. This volatility is due to the change in k_{eff} approaching the uncertainty in the original k_{eff}. The most reliable results were from the 1% and 2% perturbations.

As with the homogenous model, the total uranium-235 atom density was perturbed by 2%, 1%, 0.5%, and 0.25%. Again, for accurate results, a Δk of ~0.009001 was desired. The uranium-235 was spread across three separate fuel sections, and due to this, each section was perturbed by the same percentage. Table 16 shows the sensitivity parameters for the first-order perturbations in the heterogeneous system.

Table 16. Sensitivity parameters for Direct Perturbations in the Heterogeneous System

Atom Density Perturbations	Average Δk	Sensitivity Parameter	Difference in Sensitivity Parameter (%)
TSUNAMI		0.17404	
2%	0.00649	0.18003	-2.22
1%	0.00313	0.17837	-1.31
0.5%	0.001625	0.18367	-4.34
0.25%	0.000815	0.18090	-2.77

The desired Δk of 0.009001 was most closely achieved by the 2% perturbation and provides a sensitivity parameter within 2%, which is similar to the homogeneous model. Similar to the homogeneous model, as the perturbation shrunk, their reliability dwindled and became unpredictable. Both the heterogeneous and homogeneous first-order perturbation models provide confidence the TSUNAMI calculations are working correctly, and the results obtained are correct.

5.4 SCALE Homogenization

To determine the effects of homogenization on the cross-section uncertainty, a heterogeneous and homogeneous model were run in SCALE. The two models were then compared to determine the homogenization effect on the sensitivities for cross-sections, as well as on k_{eff}. For both systems, continuous energy cross-section sets along with the IFP method were utilized for calculating the sensitivity coefficients.

For the heterogeneous model, the top ten nuclide cross-section sensitives were selected for analysis. These cross-sections were determined to be the most sensitive in the subassembly, and were the most important neutron interactions in the system. Table 17 shows the energy, region, and mixture integrated sensitivity coefficients for the top ten nuclide cross-sections. Along with this, Figure 25 gives a graphical representation of Table 17, which shows the

sensitivities relative to each other and provides context for the largest sensitivity values. The sensitivity per unit lethargy scales parameters which have broad energy groups. Parameters with broad energy groups would show a large sensitivity response since their energy domains encompass multiple narrow energy domains for different parameters. The scaling factor takes the original sensitivity value and divides by the natural log of the upper energy bound divided by the lower energy bound.

Table 17. The Energy, Region, and Mixture Integrated Sensitivity Coefficients for the Heterogeneous Model

Nuclide	Reaction	Sensitivity	Standard Deviation	Standard Deviation (%)
Na-23	Total	-6.56e-2	1.68e-3	2.56
Na-23	Elastic	-4.88e-2	1.66e-3	3.4
U-235	Total	1.78e-1	8.77e-4	0.49
U-235	Fission	3.33e-1	2.76e-4	0.08
U-235	Capture	-1.41e-1	8.38e-5	0.06
U-235	n, gamma	-1.40e-1	8.37e-5	0.06
U-235	Nu-bar	9.71e-1	7.42e-5	0.01
U-238	Total	-3.72e-2	6.09e-4	1.64
U-238	Capture	-3.81e-2	2.57e-5	0.07
U-238	n, gamma	-3.80	2.57e-5	0.07

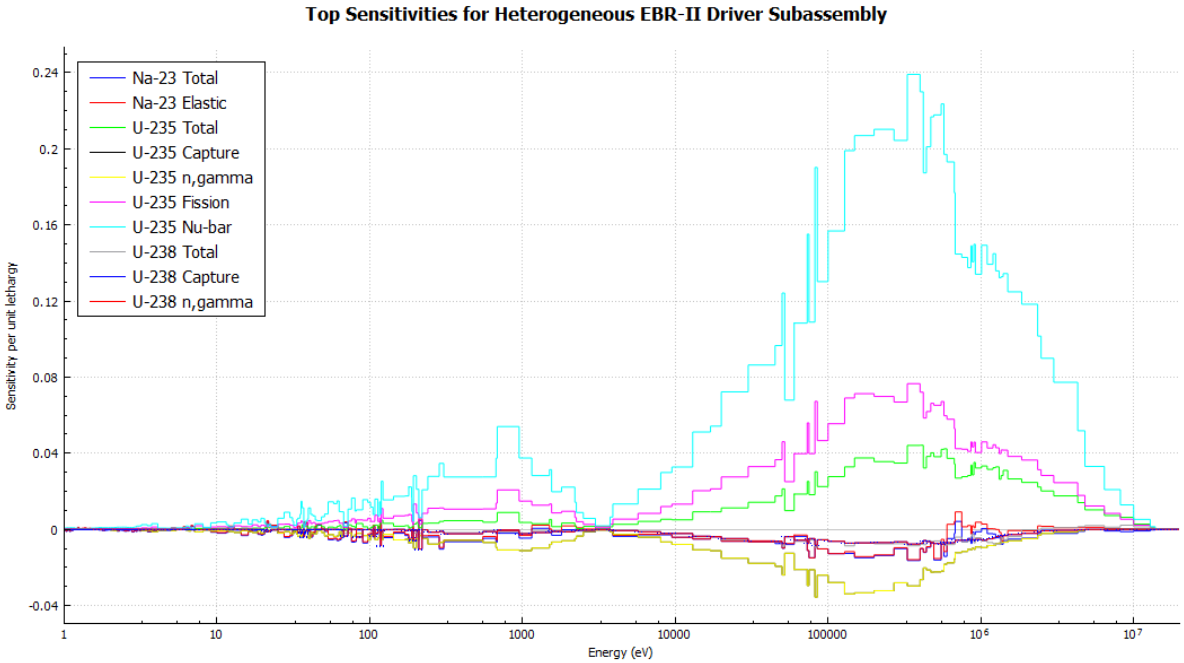

Figure 25. The energy, region, and mixture integrated sensitivity coefficient plot for the heterogeneous model.

For the homogenous model, the top ten nuclide cross-section sensitivities were selected for analysis. It was determined these sensitivities were reflective of the most important neutron interactions within the subassembly. Table 18 shows the energy, region, and mixture integrated sensitivity coefficients for the top ten nuclide cross-sections. Along with this, Figure 26 gives a graphical representation of Table 18, which shows the sensitivities relative to each other and provides context for the largest sensitivity values.

Table 18. The Energy, Region, and Mixture Integrated Sensitivity Coefficients for the Homogeneous Model

Nuclide	Reaction	Sensitivity	Standard Deviation	Standard Deviation (%)
Na-23	Total	-6.31e-2	1.62e-3	2.94
Na-23	Elastic	-4.68e-2	1.61e-3	3.44
U-235	Total	1.73e-1	8.57e-4	0.49
U-235	Fission	3.29e-1	2.75e-4	0.08
U-235	Capture	-1.39e-1	2.75e-4	0.06
U-235	n, gamma	-1.39e-1	2.75e-4	0.06
U-235	Nu-bar	9.7e-1	7.47e-5	0.01
U-238	Total	-3.798e-2	6.24e-4	1.65
U-238	Capture	-3.79e-2	2.58e-5	0.07
U-238	n, gamma	-3.78e-2	2.57e-5	0.07

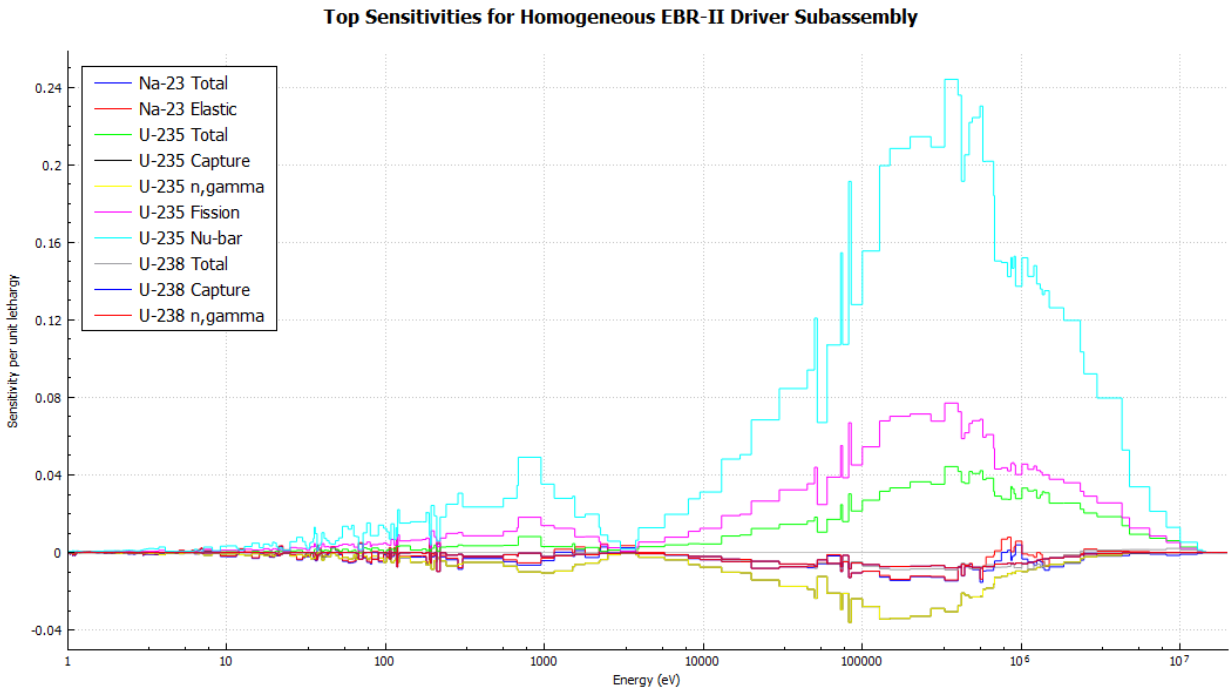

Figure 26. The energy, region, and mixture integrated sensitivity coefficient plot for the homogenized model.

To determine the effect of the homogenization process on the system overall, the difference in the sensitives were determined along with the broad effect on k_{eff}. Table 19 shows the difference in the sensitivity values due to the homogenization process. Figure 27 provides both the heterogeneous and homogeneous sensitivities for the total cross-sections of sodium-23, uranium-235, and uranium-238.

Table 19. Sensitivity Difference Due to Homogenization

Nuclide	Reaction	Sensitivity Difference	Sensitivity Difference (%)
Na-23	Total	-2.57e-3	-3.91
Na-23	Elastic	-2.00e-3	-4.10
U-235	Total	4.32e-3	2.43
U-235	Fission	4.53e-3	1.36
U-235	Capture	-1.31e-3	-0.932
U-235	n, gamma	-1.33e-3	-0.947
U-235	Nu-bar	5.40e-4	0.0556
U-238	Total	6.02e-4	1.62
U-238	Capture	-2.01e-4	-0.527
U-238	n, gamma	-2.03e-4	-0.534

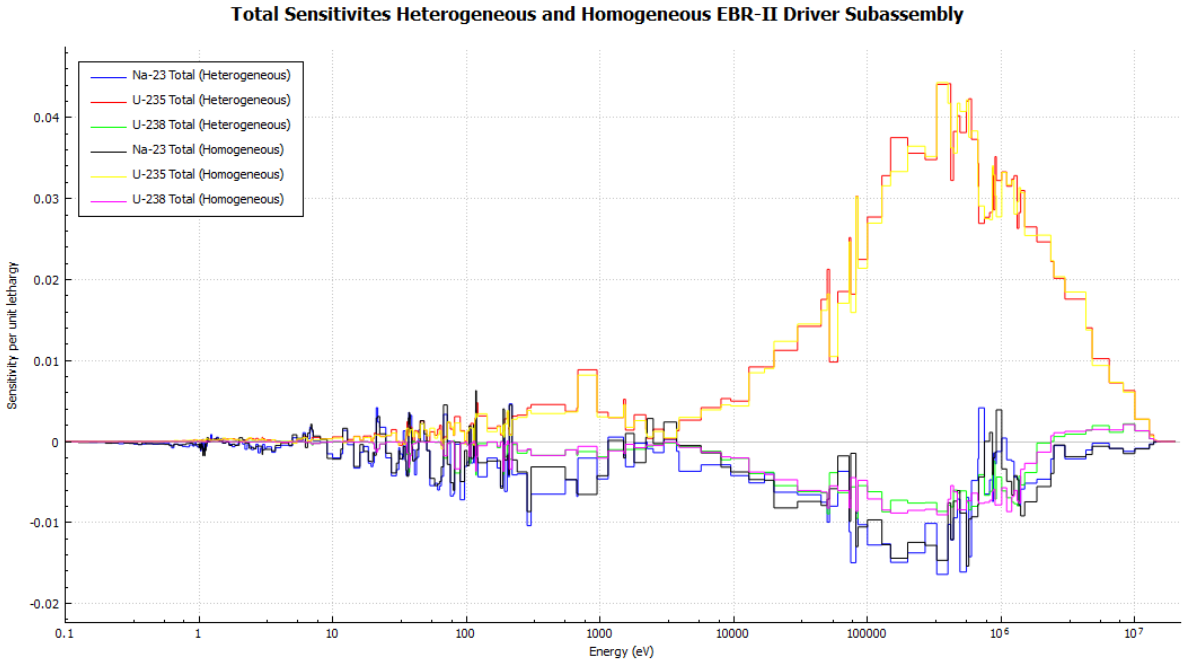

Figure 27. The energy, region, and mixture integrated sensitivity coefficient plot for the total cross-sections for the heterogeneous and homogeneous model.

Uranium-235 was the most sensitive parameter in the EBR-II driver subassembly in both the heterogeneous and homogeneous model. Due to its importance, Figure 28 shows the heterogeneous and homogeneous sensitives for uranim-235.

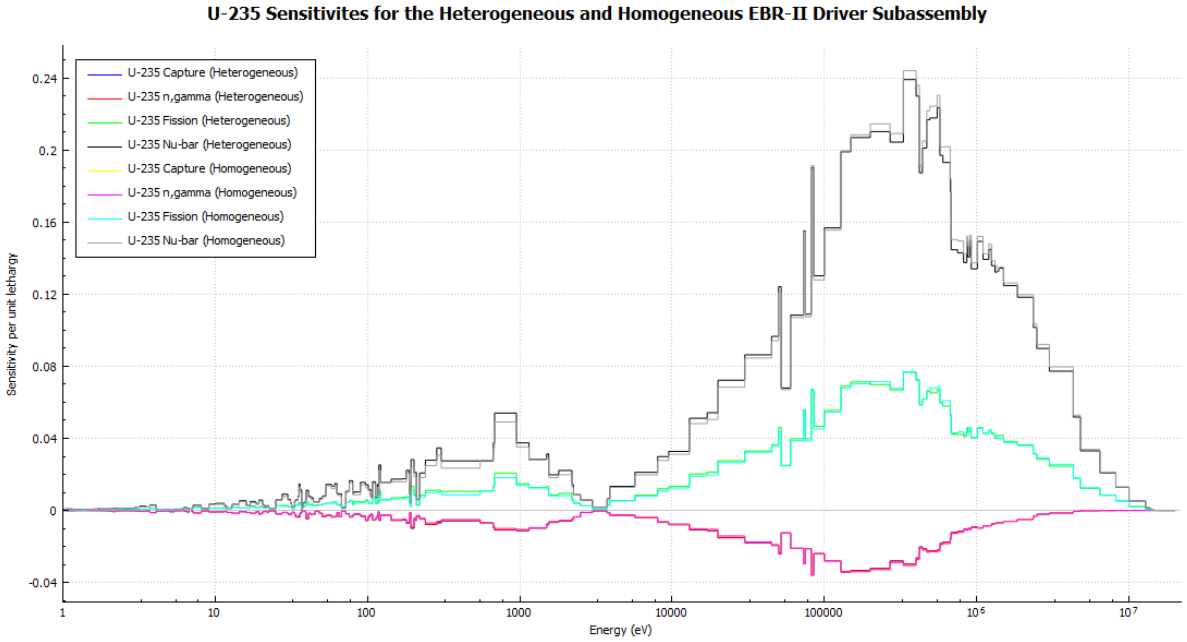

Figure 28. The energy, region, and mixture integrated sensitivity coefficient plot for the uranium-235 cross-sections for the heterogeneous and homogeneous model.

The last thing to examine in the SCALE simulation are the results tables from both runs. The results tables provide information on various reactor physics parameters including k_{eff}, average lethargy of fission, system nu-bar, and mean free path of the system. Table 20 shows both the individual homogeneous and heterogeneous results table, as well as the comparative results.

Table 20. Heterogeneous and Homogeneous SCALE Results

	Heterogeneous Results	Heterogeneous Uncertainty	Homogeneous Results	Homogeneous Uncertainty	Difference (%)
k_{eff}	1.802542	9.0e-5	1.814643	8.9e-5	0.67133
Energy of Average Lethargy of Fission (eV)	1.09e5	33.4	1.17E5	35.4	8.1293
System Nu-bar	2.49652	1.36E-5	2.49785	1.34E-5	0.053274
System Mean Free Path (cm)	6.73526	3.49E-4	6.66328	3.58E-4	-1.0687

As mentioned in section 2.2, the homogenization effect plays a role in the underlying physics occurring in the fuel assembly. It is important to remember for the SCALE analysis, the EBR-II subassembly is surrounded by a perfect reflector on all sides, which impacts the results. Despite this, there are some conclusions which can be drawn. Table 20 shows an 8% increase in the average lethargy from neutrons causing fission. The energy of average lethargy of fission is used by KENO to determine the neutron energy spectrum of a system [18]. For a system with an energy of average lethargy of fission greater than 100keV, fast neutrons are causing a majority of the fission in the system. This draws upon the fact that the atom density for uranium-235 is on the same order of magnitude as both iron and sodium. Since they are all smeared throughout the core region, there is a large probability of interacting with uranium-235 before undergoing scattering from sodium or iron and losing energy. Alternatively, in the heterogeneous model, neutrons had the opportunity to interact with both the coolant and the cladding separately from the fuel and potentially absorb neutrons before they get a chance to interact with the fuel.

The other important note is the decrease in the mean free path due to homogenization. For the perfectly reflected model, there was a 1% drop in in the mean free path. This is predominantly due to the increase in overall density for the system. As shown in Table 5, sodium encompasses approximately 40% of the volume in the driver subassembly. The sodium density in the heterogeneous model is 0.8590 g/cm^3; for the homogenized material the density is 6.9419 g/cm^3. This drastic increase in density increases the probability of interaction, which in turn decreases the mean free path. Overall, the sensitivity analysis of the driver subassembly provided the information that the homogenization process does not significantly impact the top ten sensitivity coefficients for a single driver subassembly. Despite this, the homogenization process does have a greater impact on the EBR-II core as a whole.

6.0 Summary and Conclusions

The process of modeling the EBR-II core for a reactor physics benchmark analysis required a very in depth model to be created and perturbed. Due to the extreme complexity and detail required to adequately describe the EBR-II core, it was quickly realized a much simpler model was required for future users to perturb, which would yield comparable results to the detailed model. This process required homogenizing different sections of the EBR-II core to determine their effect on k_{eff}, and to determine if the homogenization process retained the fundamental physics occurring inside EBR-II during run 138B.

Throughout the homogenization process it was determined that, except for the driver subassemblies, homogenizing the EBR-II core most likely did not fundamentally affect the most important physics occurring within the core. The homogenization results provide

evidence that the most sensitive subassemblies of the core were the driver subassemblies, and the homogenization process could be carried out on the remainder of the core with a bias in place and retain the characteristics of EBR-II. The MCNP model of homogenization provided the information that homogenization did affect k_{eff} and control rod worth values and consequently, a bias must be provided to account for this effect. Along with this, MCNP provided the confidence that the homogenization process did not affect the mean free path and flux weighted energy as a function of distance from the center of the core, it only affected the magnitude. This result was then verified using the SCALE model of an EBR-II driver assembly. The SCALE model provided confidence that most important isotopes, neutronically, retained their importance and sensitives throughout the homogenization process.

To properly correspond the homogenized and heterogeneous models, a bias was determined to be necessary. This bias was found by taking the difference between the detailed model and the homogenized model for either the critical or subcritical configurations. To be most useful, a bias was found for each integrated step of the homogenization process. These values are found in Table 21.

Table 21. Bias Values for the Integral Homogenization of the EBR-II Core.

Homogenization Step	k_{eff} Bias
Step 1 Critical	0.00567
Step 1 Subcritical	0.00564
Step 2 Critical	0.01746
Step 2 Subcritical	0.01702
Step 3 Critical	0.01351
Step3 Subcritical	0.01262
Step 4 Critical	0.02108
Step 4 Subcritical	0.02078
Step 5 Critical	0.12011
Step 5 Subcritical	0.12420

Each step for the integral homogenization is shown in Table 21**,** and it can be seen that step 5 has a large k_{eff} bias. The bias for step 5 is too large to provide information related to the EBR-II core and should not be utilized. Along with this, step 4 homogenization of the half-worth driver subassemblies, should also not be utilized due to the effect homogenization has on fueled subassemblies.

It is noted that these values were derived from the critical and subcritical control rod configurations for run 138B. These biases can be applied to any critical configuration and retain accurate results for comparison. This was tested by taking the high worth control subassembly, 05E03, which was originally at 3.01 cm and bringing it down to 0.0 cm. The change in $k_{eff,}$ from both the heterogeneous and homogeneous models was within approximately 1%. From this, it can be confidently stated that the appropriate bias factor, along with the specified homogenized model, can accurately describe the EBR-II core and could be used for future research in LMFR technology.

Bibliography

[1] C. Westfall, *Vison and Reality: The EBR-II Story*, Nuclear News, 2004, pp. 25-35.

[2] M. Lineberry, D. Pedersen, L. Walters and J. Cahalan, "Advances by the Integral Fast Reactor Program," in *American Power Conference*, Argonne, 1991.

[3] C. Pope, "Experimental Breeder Reactor II Benchmark Evaluation," Idaho State University, Pocatello, ID, 2015.

[4] F. Metcalf, J. Natoce, W. T. F. Rupp and E. Hutter, in *EBR-II System Design Descriptions*, vol. II Primary System, Argonne, Argonne National Laboratory, 1971, pp. 2.1-1 - 2.12-21.

[5] C. Till and C. Yoon, Plentiful Energy: The Story of the Integral Fast Reactor, CreateSpace, 2011.

[6] *EBR-II Control Room Console Logs*, vol. 384, 1985.

[7] "International Handbook of Evaluated Reactor Physics Benchmark Experiments," NEA/NSC/OECD, 2015.

[8] T. e. a. Goorley, "Initial MCNP6 Release Overview," *Nuclear Technology*, vol. 180, pp. 298-315, (Dec 2012).

[9] W. Yang, "Fast Reactor Physics and Computational Methods," *Nuclear Engineering and Technology*, vol. 44, no. 2, pp. 177-198, March 2012.

[10] "Average Logarithmic Energy Decrement," Nuclear Power, 2017.

[11] J. Duderstadt and J. Hamilton, "Nuclear Reactor Analysis," John Wiley & Sons, 1976, pp. 315-439.

[12] K. Okumura, Y. Oka and Y. Ishiwatari, "An Advanced Course in Nuclear Engineering," in *Nuclear Reactor Design: Nuclear Reactor Design*, Springer, 2014, pp. 60-65.

[13] J. Lamarsh and A. Baratta, Introduction to Nuclear Engineering, 3rd Edition ed., Upper Saddle River, New Jersey: Prentice Hall, 2001.

[14] "Benchmark for Neutronic Analysis of Sodium-cooled Fast Reactor Cores with Various Fuel Types and Core Sizes," Nuclear Energy Agency, Organization for Economic Co-operation and Development, 2016.

[15] M. Tatsumi, A. Yamamoto, S. Kosaka and E. Saji, "A Study in the Effects of Pin Cell Homogenization in an Actual Reactor Core Geometry," Nuclear Fuel Industires, Ltd., Osaka.

[16] R. Hwang, "Neutron Resonance Theory for Nuclear Reactor Applications: Modern Theory and Practices.," Argonne National Laboratory, Argonne, 2016.

[17] R. Murray and K. Holbert, Nuclear Energy: An Introduction to the Concepts, Systems, and Applications of Nuclear Processes, Oxford, UK: Elsevier, 2014.

[18] B. Rearden and M. Jessee, "SCALE Code System," Oak Ridge National Laboratory, Oak Ridge, TN, 2016.

[19] R. Lell, J. Morman and C. Pope, "Range of Applicability Determination for Validation of LiCl-KCl Fissile Mixtures with Sparse Benchmark Data," *Integrating Criticality Safety into the Resurgance of Nuclear Power*, 19-22 September 2005.

[20] B. Rearden, M. Williams, M. Jessee, D. Mueller and D. Wiarda, "Sensitivity and Uncertainty Analysis Capabilities and Data in SCALE," *Nuclear Technology,* pp. 236-245, 2011.

[21] J. Favorite, B. Kiedrowski and C. Perfetti, "Adjoint-Based Sensitivity and Uncertainty Analysis for Density and Composition: A User's Guide," in *Transactions of the American Nuclear Society*, Las Vegas, 2016.

[22] J. Taylor, An Introduction to Error Analysis, University Science Books, 1997.

[23] B. Rearden, C. Perfetti and L. Petrie, "Tsunami-3D: Control Module for Three Dimensional Cross Section Sensitivity and Uncertainty Analysis for Criticality," Oak Ridge National Laboratory, Oak Ridge, 2015.

[24] E. Jones, W. Marshall, B. Rearden, M. Dunn and G. Maldonado, "A Case Study in the Application of TSUNAMI-3D - Part 2, Continuous Energy," in *Transactions of the American Nuclear Society*, Las Vegas, 2016.

[25] T. Fei, A. Mohamed and T. Kim, "Neutronics Benchmark Specifications for EBR-II Shutdown Heat Removal Test SHRT-45R," Argonne National Laboratory, 2013.

[26] C. Pope, "Detailed Model Report," Idaho State University, Pocatello, ID, 2016.

[27] J. Sheppard, *EBR-II Fuel Depletion Analysis Using SCALE6.1 TRITON, T6-DEPL Sequence,* 2016.

[28] E. Ryan and C. Pope, "Sensitivity Analysis of an Experimental Breeder Reactor II Fuel Assembly," in *Transactions of the American Nuclear Society*, Las Vegas, 2016.

[29] B. Wendt and J. Lehmer, "Plexi Configuration and Operation," RISE Complex, Pocatello, 2016.

[30] D. Pelowitz, "MCNP6 User's Manual," Los Alamos National Laboratory, Los Alamos, 2013.

[31] *MATLAB R2016b,* Natick, MA: The MathWorks Inc., 2016.

[32] B. Rearden and M. E. Jessee, *SCALE Code System, ORNL/TM-2005/39, Version 6.2.1,* Oak Ridge, Tennessee, 2016.

[33] W. Marshall, E. Jones, B. Rearden and M. Dunn, "A Case Study in the Application of TSUNAMI-3D - Part 1, Multigroup," in *Transactions of the American Nuclear Society,* Las Vegas, NV, 2016.

Appendix A: Burnup

The burn up calculations draw from the ARC data provided by Argonne National Laboratory [25]. These data are taken into MICKA and used to swell the fuel pins and fuel elements. This was the only swelling performed for the EBR-II core and correlates with the burnup amount, where the burnup can be seen in Figure 29.

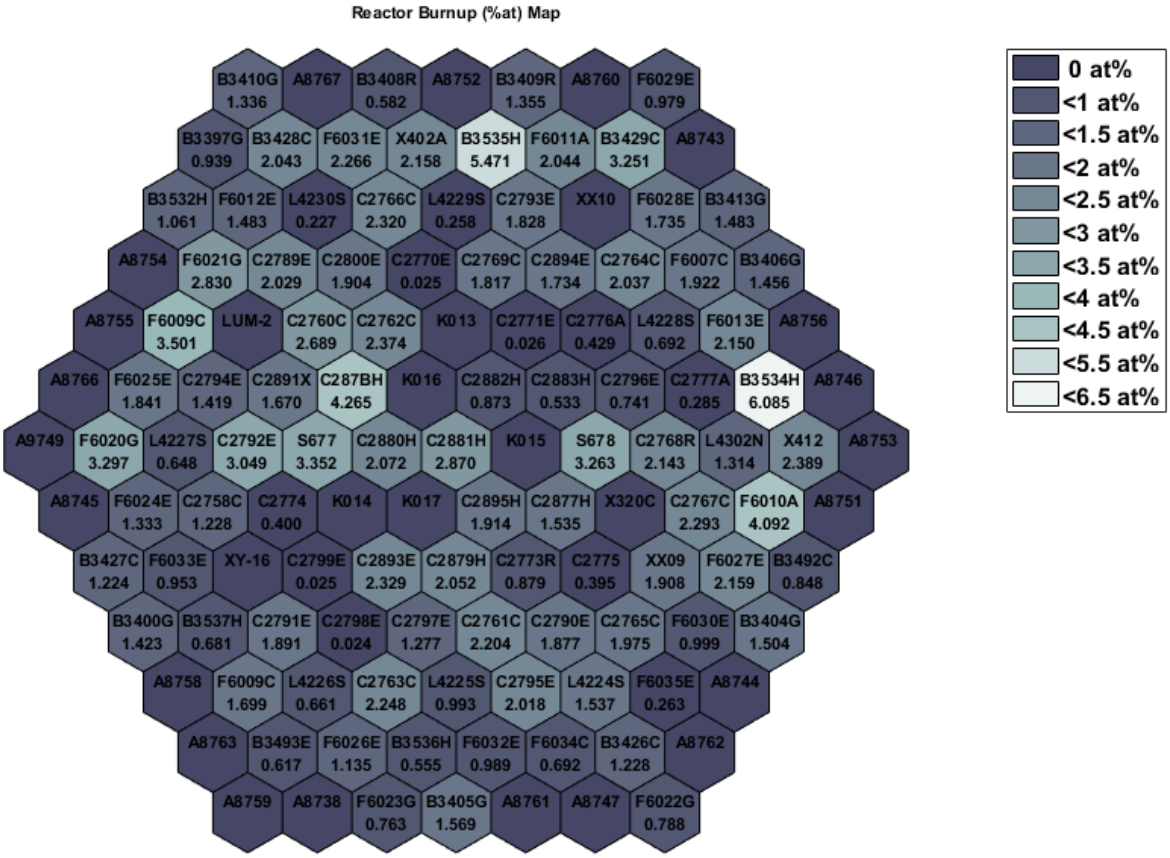

Figure 29. Burnup map for EBR-II core.

Appendix B: SCALE Atom Densities for Homogenization

A sample of the homogenization process is shown for the SCALE input file. This format was followed for all of the MCNP homogenization processes as well. Table 22 provides the heterogeneous atom densities, while Table 23 provides the homogenized atom densities.

Table 22. Material Atom Densities for Heterogeneous Materials

Upper Fuel Pin		Middle Fuel Pin		Bottom Fuel Pin		Stainless Steel		Sodium	
ZAID	at%	ZAID	at%	ZAID	at%	ZAID	at%	ZAID	at%
38090	1.53E-04	38090	1.62E-04	38090	1.62E-04	6012	3.19E-04	11023	2.52E-02
40092	1.96E-04	40092	2.03E-04	40092	2.03E-04	6013	3.45E-06		
40093	1.66E-04	40093	1.76E-04	40093	1.76E-04	14028	1.59E-03		
40094	2.04E-04	40094	2.12E-04	40094	2.12E-04	14029	8.07E-05		
40096	1.68E-04	40096	1.77E-04	40096	1.77E-04	14030	5.32E-05		
42092	7.35E-04	42092	6.88E-04	42092	6.88E-04	15031	7.03E-05		
42094	4.49E-04	42094	4.21E-04	42094	4.21E-04	24050	6.87E-04		
42095	8.13E-04	42095	7.68E-04	42095	7.68E-04	24052	1.32E-02		
42096	7.99E-04	42096	7.49E-04	42096	7.49E-04	24053	1.50E-03		
42097	6.04E-04	42097	5.84E-04	42097	5.84E-04	24054	3.74E-04		
42098	1.28E-03	42098	1.22E-03	42098	1.22E-03	25055	1.76E-03		
42100	5.99E-04	42100	5.80E-04	42100	5.80E-04	26054	3.31E-03		
43099	1.52E-04	43099	1.61E-04	43099	1.61E-04	26056	5.19E-02		
44096	1.99E-04	44096	1.86E-04	44096	1.86E-04	26057	1.20E-03		
44099	4.43E-04	44099	4.15E-04	44099	4.15E-04	26058	1.60E-04		
44100	4.40E-04	44100	4.13E-04	44100	4.13E-04	26058	6.73E-03		
44101	7.08E-04	44101	6.78E-04	44101	6.78E-04	28060	2.59E-03		

44102	1.18E-03	44102	1.12E-03	44102	1.12E-03	28061	1.13E-04
44104	6.68E-04	44104	6.31E-04	44104	6.31E-04	28062	3.59E-04
45103	5.20E-04	45103	4.92E-04	45103	4.92E-04	28064	9.15E-05
54134	1.44E-04	54134	1.52E-04	54134	1.52E-04	42092	1.86E-04
55133	1.18E-04	55133	1.24E-04	55133	1.24E-04	42094	1.16E-04
55135	1.20E-04	55135	1.27E-04	55135	1.27E-04	42095	2.00E-04
55137	1.12E-04	55137	1.18E-04	55137	1.18E-04	42095	2.10E-04
57139	1.13E-04	57139	1.20E-04	57139	1.20E-04	42097	1.20E-04
58142	9.97E-05	58142	1.06E-04	58142	1.06E-04	42098	3.05E-04
60148	2.83E-05	60148	2.99E-05	60148	2.99E-05	42100	1.22E-04
92234	1.25E-06	92234	1.06E-06	92234	1.06E-06		
92235	1.79E-02	92235	1.80E-02	92235	1.80E-02		
92236	1.95E-04	92236	1.71E-04	92236	1.71E-04		
92238	9.21E-03	92238	9.23E-03	92238	9.23E-03		
93237	2.43E-06	93237	1.94E-06	93237	1.94E-06		
94236	4.10E-12	94236	2.77E-12	94236	2.77E-12		
94238	2.80E-08	94238	1.98E-08	94238	1.98E-08		
94239	5.41E-05	94239	4.73E-05	94239	4.73E-05		
94240	1.96E-07	94240	1.49E-07	94240	1.49E-07		
94241	6.12E-10	94241	4.04E-10	94241	4.04E-10		
95241	4.88E-12	95241	3.20E-12	95241	3.20E-12		
95242	6.50E-15	95242	3.71E-15	95242	3.71E-15		
95243	2.17E-15	95243	1.08E-15	95243	1.08E-15		

96242	1.86E-14	96242	1.06E-14	96242	1.06E-14
96243	1.13E-17	96243	5.61E-18	96243	5.61E-18
96244	8.01E-18	96244	3.46E-18	96244	3.46E-18
96245	1.57E-21	96245	6.44E-22	96245	6.44E-22
96246	1.15E-25	96246	4.21E-26	96246	4.21E-26

Table 23. Atom Densities for Homogenized Material

Homogenized Material	
ZAID	at%
6012	5.84E-03
6013	6.32E-05
11023	9.23E-01
14028	2.91E-02
14029	1.48E-03
14030	9.76E-04
15031	1.29E-03
24050	1.26E-02
24052	2.43E-01
24053	2.75E-02
24054	6.85E-03
25055	3.23E-02
26054	6.07E-02
26056	9.52E-01
26057	2.20E-02
26058	2.93E-03
28058	1.23E-01
28060	4.75E-02
28061	2.07E-03
28062	6.59E-03
28064	1.68E-03
38090	6.48E-03
40092	8.15E-03
40093	7.01E-03
40094	8.50E-03
40096	7.08E-03

42092	3.20E-02
42094	1.96E-02
42095	3.55E-02
42096	3.50E-02
42097	2.62E-02
42098	5.59E-02
42100	2.61E-02
43099	6.43E-03
44096	7.75E-03
44099	1.72E-02
44100	1.71E-02
44101	2.80E-02
44102	4.64E-02
44104	2.62E-02
45103	2.04E-02
54134	6.09E-03
55133	4.97E-03
55135	5.06E-03
55137	4.71E-03
57139	4.79E-03
58142	4.21E-03
60148	1.20E-03
92234	4.55E-05
92235	7.31E-01
92236	7.28E-03
92238	3.75E-01
93237	8.55E-05
94236	1.31E-10
94238	9.17E-07
94239	2.01E-03
94240	6.69E-06
94241	1.92E-08
95241	1.53E-10
95242	1.89E-13
95243	5.85E-14
96242	5.40E-13
96243	3.05E-16
96244	2.02E-16
96245	3.88E-20
96246	2.70E-24

Appendix C: MATLAB Progression

The process of altering a large MATLAB code came with its difficulties and lessons learned. To aide in future work, or work of a similar nature, a brief description of the lessons learned are provided.

1. Generalization is the key to quick coding.

Many of the functions created for the homogenization process were needed for each step of the process with only minor changes. This meant many of the functions could remain constant if the variables within were constant, and only the variables fed into the function were altered.

2. Avoid using i, j, or k for looping variables

It is easy to want to use a singular letter when looping in functions, however, this can lead to MATLAB trying to overwrite pre-defined functions which can wreak havoc. It is often best to use double letters such as ii, jj, or kk for loops to prevent trying to overwrite functions.

3. Sub-functions greatly increase optimization in MATLAB.

MATLAB runs better with multiple sub-functions running loops rather than with just one large function trying to run multiple loops. A general guideline: if a function is needed more than once, or if a function is going across multiple other functions, make a sub-function out of it. This will not only decrease run time, but it will also increase the generalization ability of the program.

4. Make logical naming choices persistent throughout the code.

To ensure ease of code altering, ensure the names of variables are well defined. Create acronyms for systems and stick to it. If a variable is going to be made throughout the program, consider making it a global variable, or at least a persistent variable to ease having to recreate the variable later.

5. Validation and verification are key.

To prevent errors and a lengthy verification process later on, build in a debugging system as you go to check your work. This will save time later on, but is not a substitute for hand verification of results. Hand written verification will provide confidence the program is operating and performing calculations correctly.

Appendix D: Sample MCNP Input File for the Heterogeneous Model

The partial input file shown in Figure 30, Figure 31, and Figure 32 is for the heterogeneous model which provided the reference for homogenization. This section of input file contains the cell, surface and material cards for the driver subassembly 04E01.

Figure 30. MCNP cell cards for the heterogeneous driver subassembly 04E01.

```
c ********************************************************************************
c ***************** Driver MKIIA M#26 POS:04E01 ID:C2790E ********************
c ********************************************************************************
c
427      5 0.084823 -26 1105 1104 1106 1107  U=26 IMP:N=1              $ Hex Duct
433      1 0.023306 26 -1103  U=26 IMP:N=1                          $ INF Na for Lat
428      11 0.088664 -1104  U=26 IMP:N=1                           $ Homog Upper Ext
429      1 0.023306 -1105 1109  U=26 IMP:N=1                        $ Sodium coolant
c
c ************************** Pin: 1 Sec: 1 of SA: 26 **************************
c
420      26006 0.082692684 -1111 1112  U=26002 IMP:N=1                $ Pin: 1  Cladding
421      4 6.762e-05 1100 -1112  U=26002 IMP:N=1                     $ Pin: 1  Plenum Gas
422      26001 0.036601 -1113 1101  U=26002 IMP:N=1                   $ Pin: 1  Fuel Slug
Sec 1
423      26002 0.036609 -1113 -1101 1102  U=26002 IMP:N=1             $ Pin: 1  Fuel Slug
Sec 2
424      26003 0.036587 -1113 -1102  U=26002 IMP:N=1                  $ Pin: 1  Fuel Slug
Sec 3
425      1 0.023306 -1100 -1112 1113  U=26002 IMP:N=1                 $ Pin: 1  Sodium
426      8 0.085931 -1114  U=26002 IMP:N=1                          $ Pin: 1  Wire Wrap
436      1 0.023306 -1103 1111 1114  U=26002 IMP:N=1                 $ Fuel Pin Cell
c
c ***************************** Pin Lattice Cards ****************************
c
434      1 0.023306 -1110 Lat=2 U=26001 IMP:N=1                     $ Element Lattice
     fill  -7:7 -7:7 0:0
    26001 26001 26001 26001 26001 26001 26001 26001 26001 26001 26001 26001
    26001 26001 26001 26001 26001 26001 26001 26001 26001 26001 26001 26001
    26001 26001 26001 26001 26001 26001 26001 26001 26001 26001 26001 26001
    26001 26002 26002 26002 26002 26002 26002 26001 26001 26001 26001 26001
    26001 26001 26001 26002 26002 26002 26002 26002 26002 26002 26001 26001
    26001 26001 26001 26001 26001 26002 26002 26002 26002 26002 26002 26002
    26002 26001 26001 26001 26001 26001 26001 26002 26002 26002 26002 26002
    26002 26002 26002 26002 26001 26001 26001 26001 26001 26002 26002 26002
    26002 26002 26002 26002 26002 26002 26002 26001 26001 26001 26001 26002
    26002 26002 26002 26002 26002 26002 26002 26002 26002 26002 26001 26001
```

```
     26001 26001 26002 26002 26002 26002 26002 26002 26002 26002 26002 26002
     26001 26001 26001 26001 26001 26002 26002 26002 26002 26002 26002 26002
     26002 26002 26001 26001 26001 26001 26001 26001 26002 26002 26002 26002
     26002 26002 26002 26002 26001 26001 26001 26001 26001 26001 26001 26002
     26002 26002 26002 26002 26002 26002 26001 26001 26001 26001 26001 26001
     26001 26001 26002 26002 26002 26002 26002 26002 26001 26001 26001 26001
     26001 26001 26001 26001 26001 26001 26001 26001 26001 26001 26001 26001
     26001 26001 26001 26001 26001 26001 26001 26001 26001 26001 26001 26001
     26001 26001 26001 26001 26001 26001 26001 26001 26001
435      1 0.023306 -1109 fill=26001  U=26 IMP:N=1              $ Pin Lattice
430      12 0.089189 -1106  U=26 IMP:N=1                      $ Homog Lower Ext
431      1 0.023306 -26 -1107 1108  U=26 IMP:N=1               $ Na Surr Lower Ext
432      13 0.087218 -1108  U=26 IMP:N=1                      $ Lower Cyn Homog
```

Figure 31. MCNP surface cards for the heterogeneous driver subassembly 04E01.

```
c ********************************************************************************
c ***************** Driver MKIIA M#26 POS:04E01 ID:C2790E ******************
c ********************************************************************************
c
26     RHP 0 0 -113.36782 0 0 219.6084 2.9083                $ Outer Wall of Hex
Duct
1103     SO 328.77252                                        $ Surr Na For Lat
1104     RHP 0 0 65.54216 0 0 40.59682 2.8067                $ Upper Extent Inner
Hex
1105     RHP 0 0 0 0 0 65.54216 2.8067                       $ Inner Wall Hex Duct
1100     PZ 35.375492                                        $ Driver Na/He Boundary
1101     PZ 23.160332                                        $ Fuel Section Plane Sec 1/2
1102     PZ 11.580171                                        $ Fuel Section Plane Sec 2/3
1106     RHP 0 0 0 0 0 -61.3537 2.8067                       $ Lower Extent Inner Hex
1107     PZ -61.4553                                         $ Plane Separation Duct to Cylinder
1108     RCC 0 0 -61.4553 0 0 -51.91252 2.38125              $ Lower Extension
Cylinder
c
c ************************** Pin: 1 Sec: 1 of SA: 26 **************************
c
1111     RCC -0.034096778 0 1e-05 0 0 61.735999 0.22459678   $ Pin: 1 Sec # 1
Outer Cladding wall
1112     RCC -0.034096778 0 0.31751 0 0 60.732699 0.19361791 $ Pin: 1 Sec #  1
Inner cladding wall
1113     RCC -0.034096778 0 0.31851 0 0 34.740482 0.18400119 $ Pin: 1 Fuel
slug boundary
1114     RCC 0.25373 0 1e-05 0 0 61.735999 0.06223           $ Pin: 1 Wire Wrap
c
c ********************** Pin Lattice Cards for Elements **********************
c
```

```
1109     RHP 0 0 1e-05 0 0 61.736019 2.778633                    $ Element Lattice
Bounding Surface
1110     RHP 0 0 -30.868 0 0 123.472 0 0.28321 0                 $ Lattice Window
```

Figure 32. MCNP material cards for the heterogeneous driver subassembly 04E01.

```
c ********************************************************************************
c ******************** MICKA #: 26 ID: C2790E POS: 04E01 *********************
c ********************************************************************************
c
c
c ****************************** Fuel/Blanket Slug ******************************
c
c
c ********************************** Pin Sec: 1 **********************************
c
m26001 96242.00c 5.9409e-13 96243.00c 3.6224e-16
     96244.00c 2.5786e-16 96245.00c 5.0886e-20
     96246.00c 3.7346e-24 95241.00c 1.552e-10
     95242.00c 2.0741e-13 95243.00c 6.948e-14
     94236.00c 1.2773e-10 94238.00c 8.7899e-07
     94239.00c 0.0017075 94240.00c 6.2083e-06
     94241.00c 1.9474e-08 93237.00c 7.6008e-05
     92234.00c 3.8541e-05 92235.00c 0.55413
     92236.00c 0.0060847 92238.00c 0.28934
     60148.00c 0.00055239 58142.00c 0.0018663
     57139.00c 0.0020788 55133.00c 0.0020629
     55135.00c 0.0021331 55137.00c 0.0020142
     54134.00c 0.0025448 45103.00c 0.0070525
     44096.00c 0.0025181 44099.00c 0.0057849
     44100.00c 0.0057942 44101.00c 0.0094261
     44102.00c 0.015888 44104.00c 0.0091527
     43099.00c 0.0019865 42092.00c 0.0089073
     42094.00c 0.0055643 42095.00c 0.010184
     42096.00c 0.010103 42097.00c 0.0077173
     42098.00c 0.016513 42100.00c 0.0078944
     40092.00c 0.0023739 40093.00c 0.0020353
     40094.00c 0.0025277 40096.00c 0.002126
     38090.00c 0.00182
c
c ********************************** Pin Sec: 2 **********************************
c
m26002 96242.00c 5.634e-13 96243.00c 3.1467e-16
     96244.00c 2.3828e-16 96245.00c 4.4669e-20
     96246.00c 3.247e-24 95241.00c 1.4668e-10
     95242.00c 1.9659e-13 95243.00c 6.5333e-14
     94236.00c 1.694e-10 94238.00c 9.6535e-07
```

94239.00c 0.0017277 94240.00c 5.9478e-06
94241.00c 1.8412e-08 93237.00c 8.4347e-05
92234.00c 4.5484e-05 92235.00c 0.55181
92236.00c 0.0060949 92238.00c 0.28905
60148.00c 0.0006426 58142.00c 0.0021672
57139.00c 0.0024163 55133.00c 0.0024
55135.00c 0.0024817 55137.00c 0.0023427
54134.00c 0.0029576 45103.00c 0.0069748
44096.00c 0.0024419 44099.00c 0.0056088
44100.00c 0.0056299 44101.00c 0.0094656
44102.00c 0.015705 44104.00c 0.0090163
43099.00c 0.0023077 42092.00c 0.0086454
42094.00c 0.0053977 42095.00c 0.010002
42096.00c 0.0098124 42097.00c 0.0078644
42098.00c 0.016392 42100.00c 0.0080574
40092.00c 0.0026726 40093.00c 0.0023647
40094.00c 0.0028502 40096.00c 0.0024573
38090.00c 0.0021114
c
c ********** Pin Sec: 3 **********
c
m26003 96242.00c 3.3918e-13 96243.00c 1.7989e-16
96244.00c 1.1147e-16 96245.00c 2.0817e-20
96246.00c 1.3672e-24 95241.00c 1.0189e-10
95242.00c 1.1859e-13 95243.00c 3.4542e-14
94236.00c 8.6358e-11 94238.00c 6.2307e-07
94239.00c 0.0014908 94240.00c 4.711e-06
94241.00c 1.2835e-08 93237.00c 6.0687e-05
92234.00c 3.2607e-05 92235.00c 0.5596
92236.00c 0.0053168 92238.00c 0.28987
60148.00c 0.00058426 58142.00c 0.0019766
57139.00c 0.0021999 55133.00c 0.0021822
55135.00c 0.0022561 55137.00c 0.0021309
54134.00c 0.0026934 45103.00c 0.0066839
44096.00c 0.0023577 44099.00c 0.0054118
44100.00c 0.0054409 44101.00c 0.0090215
44102.00c 0.015074 44104.00c 0.0086518
43099.00c 0.002103 42092.00c 0.0083461
42094.00c 0.0052109 42095.00c 0.0096125
42096.00c 0.0094757 42097.00c 0.0074641
42098.00c 0.015703 42100.00c 0.0076446
40092.00c 0.002459 40093.00c 0.0021539
40094.00c 0.0026215 40096.00c 0.0022413
38090.00c 0.0019272
c
c ********** Fuel Sodium **********

```
c
c
c ***************************** Generic Mat # 1 Used ****************************
c
c
c ***************************** Fuel Plenum Gas *****************************
c
c
c ***************************** Generic Mat # 4 Used ****************************
c
c
c ****************************** Fuel Cladding ******************************
c
m26006 6000.00c -0.0008 14028.00c -0.0091873442
     14029.00c -0.00048317866 14030.00c -0.00032947717
     24050.00c -0.0070952674 24052.00c -0.14228892
     24053.00c -0.016445098 24054.00c -0.0041707192
     25055.00c -0.02 26054.00c -0.036933242
     26056.00c -0.6012198 26057.00c -0.014133132
     26058.00c -0.0019138254 28058.00c -0.080637567
     28060.00c -0.032131283 28061.00c -0.0014195597
     28062.00c -0.0046018049 28064.00c -0.0012097853
     42092.00c -0.0035543592 42094.00c -0.0022636567
     42095.00c -0.0039374561 42096.00c -0.0041688432
     42097.00c -0.0024117587 42098.00c -0.0061566394
     42100.00c -0.0025072868
mt26006 fe56.00t
c
c ***************************** No Poison Slug ******************************
c
c
c ***************************** Fuel Pin Wirewrap ****************************
c
c
c ***************************** Generic Mat # 8 Used ****************************
c
c
c ************************** No Poison Plenum Gas ***************************
c
c
c ***************************** No Poison Cladding ****************************
c
c
c ******************************* No Dummy Pin ******************************
c
c
```

```
c ********************************* Hex Duct ***********************************
c
c
c ***************************** Generic Mat # 5 Used ***************************
c
c
c ******************************* Duct Sodium **********************************
c
c
c ***************************** Generic Mat # 1 Used ***************************
c
c
c ************************** Smeared Upper Ext *****************************
c
c
c ***************************** Generic Mat # 11 Used ***************************
c
c
c ************************** Smeared Lower Ext *****************************
c
c
c ***************************** Generic Mat # 12 Used ***************************
c
c
c ************************** Smeared Lower Adapter *************************
c
c
c ***************************** Generic Mat # 13 Used ***************************
c
c
c ****************** No Smeared Inner Hext Duct Lower Adapter *****************
c
c
c ******************************* No Other Pins SS *****************************
c
c
c ********************************* No Pin Shield ******************************
c
c
c ********************************** No Spare **********************************
c
c
c ********************************** No Spare **********************************
c
```

Appendix E: Sample MCNP Input File for the Homogeneous Model

The partial input file shown in Figure 33, Figure 34, and Figure 35 is for the homogeneous model. In this model the blanket, reflector, dummy, half-worth driver, and driver subassemblies were all homogenized. Only the control, safety, high worth control, and experimental subassemblies retained their heterogeneous configuration. This section of input file contains the cell, surface and material cards for the driver subassembly 04E01.

Figure 33. MCNP cell cards for homogenized driver subassembly 04E01.

```
c ********************************************************************************
c ****************** Driver MKIIA M#26 POS:04E01 ID:C2790E ********************
c ********************************************************************************
c
170      5 0.084823 -21 880 883 881 882  U=26 IMP:N=1              $ Hex Duct
171      11 0.088664 -880  U=26 IMP:N=1                          $ Homog Upper Ext
172      12 0.089189 -883  U=26 IMP:N=1                          $ Homog Lower Ext
173      26001 0.035295173 -881  U=26 IMP:N=1                     $ Homog Fuel Region
174      26002 0.024381374 -882  U=26 IMP:N=1                    $ Homog Plenum Region
175      1 0.023306 -879 21 880 883 881 882  U=26 IMP:N=1          $ INF Na for
```

Figure 34. MCNP surface cards for homogenized driver subassembly 04E01.

```
c ********************************************************************************
c ****************** Driver MKIIA M#26 POS:04E01 ID:C2790E ********************
c ********************************************************************************
c
21    RHP 0 0 -61.4553 0 0 163.68652 2.9083                      $ Outer Wall of Hex Duct
880    RHP 0 0 65.85967 0 0 40.59682 2.8067                      $ Upper Extension
883    RHP 0 0 0 0 0 -61.3537 2.8067                             $ Lower Extension
881    RHP 0 0 0.31751 0 0 35.375482 2.8067                      $ Homogenized Fuel Region
882    RHP 0 0 35.692992 0 0 26.360517 2.8067                    $ Homogenized Plenum Region
879    SO 328.77252                                              $ Surr Na For Lat
```

Figure 35. MCNP material cards for homogenized driver subassembly 04E01.

```
c ********************************************************************************
c ******************** MICKA #: 26 ID: C2790E POS: 04E01 **********************
c ********************************************************************************
c
c
c ***************************** Smeared Material 1 ****************************
c
```

```
m26001 96242.00c 4.9996794e-15 96243.00c 2.8621834e-18
     96244.00c 2.0297833e-18 96245.00c 3.8875253e-22
     96246.00c 2.789021e-26 95241.00c 1.3487909e-12
     95242.00c 1.7457302e-15 95243.00c 5.6574246e-16
     94236.00c 1.2810743e-12 94238.00c 8.2424159e-09
     94239.00c 1.6454907e-05 94240.00c 5.6343719e-08
     94241.00c 1.6943309e-10 93237.00c 7.3838596e-07
     92234.00c 3.8960661e-07 92235.00c 0.005563508
     92236.00c 5.844526e-05 92238.00c 0.0029003068
     60148.00c 5.9433967e-06 58142.00c 2.0076098e-05
     57139.00c 2.2363937e-05 55133.00c 2.2197255e-05
     55135.00c 2.2951516e-05 55137.00c 2.167181e-05
     54134.00c 2.73772e-05 45103.00c 6.9183357e-05
     44096.00c 2.4443915e-05 44099.00c 5.6136798e-05
     44100.00c 5.6335539e-05 44101.00c 9.3240832e-05
     44102.00c 0.00015588567 44104.00c 8.9591759e-05
     43099.00c 2.1369166e-05 42092.00c 0.00066436068
     42094.00c 0.00043003844 42095.00c 0.0007605573
     42096.00c 0.00080540732 42097.00c 0.00049040027
     42098.00c 0.0012286109 42100.00c 0.00052192665
     40092.00c 2.5071309e-05 40093.00c 2.1892607e-05
     40094.00c 2.6721129e-05 40096.00c 2.279685e-05
     38090.00c 1.9570027e-05 11023.00c 0.013688481
     6000.00c 1.6996657e-05 14028.00c 0.00045466884
     14029.00c 2.4766167e-05 14030.00c 1.7469155e-05
     24050.00c 5.0236154e-05 24052.00c 0.0010074388
     24053.00c 0.00011643514 24054.00c 2.9529668e-05
     25055.00c 0.00014160468 26054.00c 0.000261496
     26056.00c 0.0042567769 26057.00c 0.00010006588
     26058.00c 1.3550331e-05 28058.00c 0.00057093285
     28060.00c 0.000227497 28061.00c 1.0050815e-05
     28062.00c 3.2581856e-05 28064.00c 0.00024268369
mt26001 fe56.00t
c
c ***************************** Smeared Material 2 *****************************
c
m26002 2003.00c 4.4615705e-12 2004.00c 4.3218888e-06
     18036.00c 3.9221621e-08 18038.00c 8.2063652e-09
     18040.00c 1.433119e-05 6000.00c 1.5271709e-05
     14028.00c 0.00040852565 14029.00c 2.2252711e-05
     14030.00c 1.5696255e-05 24050.00c 4.5137813e-05
     24052.00c 0.00090519641 24053.00c 0.00010461843
     24054.00c 2.6532776e-05 25055.00c 0.00012723358
     26054.00c 0.00023495743 26056.00c 0.0038247674
     26057.00c 8.9910446e-05 26058.00c 1.2175143e-05
     28058.00c 0.00051299032 28060.00c 0.00020440891
```

```
     28061.00c 9.030783e-06 28062.00c 2.9275205e-05
     28064.00c 7.6962654e-06 42092.00c 0.00051920438
     42094.00c 0.00033785398 42095.00c 0.00059393375
     42096.00c 0.00063545485 42097.00c 0.00037146162
     42098.00c 0.0009580314 42100.00c 0.00039813591
     11023.00c 0.57227786
mt26002 fe56.00t
c
c ************************** No Smeared Material 3 **************************
c
c
c ************************** No Smeared Material 4 **************************
c
c
c ************************** No Smeared Material 5 **************************
c
c
c ************************** No Smeared Material 6 **************************
c
c
c ************************** No Smeared Material 7 **************************
c
c
c ************************** No Smeared Material 8 **************************
c
c
c ************************** No Smeared Material 9 **************************
c
c
c ************************** No Smeared Material 10 *************************
c
c
c ************************** No Smeared Material 11 *************************
c
c
c ************************** No Smeared Material 12 *************************
c
c
c ************************** No Smeared Material 13 *************************
c
c
c ************************** No Smeared Material 14 *************************
c
c
c ************************** No Smeared Material 15 *************************
c
```

```
c
c ************************** No Smeared Material 16 **************************
c
c
c ************************** No Smeared Material 17 **************************
c
c
c ************************** No Smeared Material 18 **************************
c
c
c ************************** No Smeared Material 19 **************************
```

Appendix F: SCALE Input File for the Heterogeneous Model

The input file in Figure 36 is for the heterogeneous model for the SCALE sensitivity and uncertainty analysis. This model was altered from the original model created by Emerald Ryan to incorporate the IFP method and continuous cross-section sets [28].

Figure 36. SCALE input file for the heterogeneous model.

```
'EBR-II Heterogeneous Model for TSUNAMI
=tsunami-3d-k6
ebr-ii heterogenous model
ce_v7_endf
read composition
sodium 1 den=0.859 1 666 end
sodium 2 den=0.859 1 666 end
sodium 3 den=0.859 1 666 end
ss316 4 1 685 end
ss316 5 1 685 end
ss316 6 1 685 end
wtpt_emty_drv_rd 10 1.958281 10
11000 23.61659
14000 0.7638035
6000 0.06110428
24000 12.98466
25000 1.527607
26000 49.93365
28000 9.165642
42000 1.909522
2000 0.00306717
15031 0.03435791
1 685 end
wtpt_l_drv_shld 20 6.801966 9
6000 0.07826987
14000 0.9783733
15031 0.0440268
24000 16.63235
25055 1.956747
26000 63.96116
28000 11.74048
11000 2.162665
42000 2.445933
1 685 end
wtpt_l_drv_adpt 30 2.341 8
6000 0.056
14000 0.706
```

15031 0.032
24000 13.407
25055 1.411
26000 48.246
28000 6.703
11000 29.439
1 685 end
wtpt_u_drv_shld 40 4.22937 9
6000 0.071388
14000 0.892355
15031 0.040156
24000 15.17004
25055 1.78471
26000 58.33772
28000 10.70826
11000 10.76449
42000 2.230888
1 685 end
wtpt_up_adptr 50 1.344 8
6000 0.032
14000 0.396
15031 0.018
24000 7.522
25055 0.792
26000 27.07
28000 3.761
11000 60.409
1 685 end
wtpt_u-5s-bol_l 60 12.5884 45
96242 5.94092e-11
96243 3.62243e-14
96244 2.57857e-14
96245 5.08863e-18
96246 3.73464e-22
95241 1.55204e-08
95242 2.07407e-11
95243 6.94803e-12
94236 1.27735e-08
94239 0.1707527
94240 0.000620836
94238 8.78988e-05
94241 1.94741e-06
93237 0.007600827
92234 0.003854117
92235 55.41274
92236 0.6084691

92238 28.93361
60148 0.05523941
58142 0.1866272
57139 0.2078779
55133 0.2062934
55135 0.2133148
55137 0.2014157
54134 0.2544803
45103 0.7052501
44096 0.2518085
44099 0.5784915
44100 0.5794235
44101 0.9426117
44102 1.588832
44104 0.9152717
43099 0.1986506
42092 0.8907277
42094 0.556433
42095 1.018418
42096 1.010341
42097 0.7717362
42098 1.651279
42100 0.7894451
40092 0.2373928
40093 0.2035283
40094 0.2527716
40096 0.2126003
38090 0.181998
1 760 end
wtpt_u-5s-bol_m 70 12.5884 45
96242 3.3918e-11
96243 1.79886e-14
96244 1.11469e-14
96245 2.0817e-18
96246 1.36724e-22
95241 1.01895e-08
95242 1.18587e-11
95243 3.45425e-12
94236 8.63583e-09
94238 6.23066e-05
94239 0.1490784
94240 0.000471104
94241 1.28348e-06
93237 0.0060687
92234 0.003260724
92235 55.96012

92236 0.5316848
92238 28.98656
60148 0.05842599
58142 0.1976644
57139 0.2199926
55133 0.2182168
55135 0.2256111
55137 0.2130933
54134 0.2693359
45103 0.6683909
44096 0.2357708
44099 0.5411754
44100 0.5440865
44101 0.9021531
44102 1.507373
44104 0.865182
43099 0.2102986
42092 0.8346153
42094 0.5210888
42095 0.9612486
42096 0.9475664
42097 0.7464087
42098 1.570253
42100 0.7644576
40092 0.2459015
40093 0.2153931
40094 0.2621455
40096 0.2241264
38090 0.1927155
1 760 end
wtpt_u-5s-bol_u 80 12.5884 45
96242 3.3918e-11
96243 1.79886e-14
96244 1.11469e-14
96245 2.0817e-18
96246 1.36724e-22
95241 1.01895e-08
95242 1.18587e-11
95243 3.45425e-12
94236 8.63583e-09
94238 6.23066e-05
94239 0.1490784
94240 0.000471104
94241 1.28348e-06
93237 0.0060687
92234 0.003260724

92235 55.96013
92236 0.5316848
92238 28.98656
60148 0.05842599
58142 0.1976644
57139 0.2199926
55133 0.2182168
55135 0.2256111
55137 0.2130933
54134 0.2693359
45103 0.6683909
44096 0.2357708
44099 0.5411754
44100 0.5440865
44101 0.9021531
44102 1.507373
44104 0.865182
43099 0.2102986
42092 0.8346153
42094 0.5210888
42095 0.9612486
42096 0.9475664
42097 0.7464087
42098 1.570253
42100 0.7644576
40092 0.2459015
40093 0.2153931
40094 0.2621455
40096 0.2241264
38090 0.1927155
1 760 end
sodium 88 1 300 end
sodium 99 1 300 end
end composition
read celldata
latticecell triangpitch fuelr=0.1905 60 cladr=0.22761 4 hpitch=0.56642 1 end
latticecell triangpitch fuelr=0.1905 70 cladr=0.22761 5 hpitch=0.56642 2 end
latticecell triangpitch fuelr=0.1905 80 cladr=0.22761 6 hpitch=0.56642 3 end
end celldata
read parameter
gen=6500
npg=5000
nsk=500
htm=no
cet=2
cfp=5

```
end parameter
read geometry
unit 2
com="sodium void - driver subassembly"
rhexprism 1 0.28298 36.65 0
media 1 1 1 vol=75.32919
boundary 1
unit 11
com="depletion driver rod"
cylinder 1 0.1905 12.21666 0 origin x=-0.06 y=0 z=0
cylinder 2 0.1905 24.43334 12.21666 origin x=-0.06 y=0 z=0
cylinder 3 0.1905 36.65 24.43334 origin x=-0.06 y=0 z=0
'cladding
cylinder 4 0.221 36.65 0 origin x=-0.06 y=0 z=0
'sodium surrounding
rhexprism 5 0.28298 36.65 0
'wire wrap pin
cylinder 6 0.06223 36.65 0 origin x=0.22323 y=0 z=0
'first fuel section
media 60 1 1 vol=126.746
'cladding
media 4 1 -1 -2 -3 4 vol=108.229
'wire wrap
media 4 1 6 vol=40.57558
'sodium inside hexduct
media 1 1 5 -6 -4 vol=372.5777
'second fuel section
media 70 1 2 vol=126.746
'third fuel section
media 80 1 3 vol=126.746
boundary 5
global unit 150
com="driver subassembly - depletion"
'inner hexduct
hexprism 1 2.8067 36.65 0
array 11 1 place 7 7 1 0.06 0 0
'outer hexduct
hexprism 2 2.9083 36.65 0
'outer sodium
hexprism 9 2.9464 78 -28
hexprism 10 2.95 79 -29
'upper smeared section
hexprism 11 2.9083 78 36.65
'lower smeared section
hexprism 12 2.9083 0 -28
'hexduct
```

```
media 4 1 -1 2
'upper smear
media 88 1 11
'lower smear
media 99 1 12
'sodium inside array
media 1 1 9 -2 -11 -12
'sodium outside array
media 1 1 10 -9
boundary 10
end geometry
read array
ara=11 nux=13 nuy=13 nuz=1 typ=rhexagonal
com="
fill
11 11 11 11 11 2 2 2 11 11 11 11 11
11 11 11 2 2 11 11 11 2 2 11 11 11
11 2 2 11 11 11 11 11 11 11 2 2 11
2 11 11 11 11 11 11 11 11 11 11 11 2
2 11 11 11 11 11 11 11 11 11 11 11 2
2 11 11 11 11 11 11 11 11 11 11 11 2
2 11 11 11 11 11 11 11 11 11 11 11 2
2 11 11 11 11 11 11 11 11 11 11 11 2
2 11 11 11 11 11 11 11 11 11 11 11 2
2 2 11 11 11 11 11 11 11 11 11 2 2
11 11 2 2 11 11 11 11 11 2 2 11 11
11 11 11 11 2 2 11 2 2 11 11 11 11
11 11 11 11 11 11 2 11 11 11 11 11 11 end fill
end array
read bnds
body=10
all=mirror
end bnds
end data
read sams
end sams
end
```

Appendix G: SCALE Input File for the Homogeneous Model

The input file in Figure 37 is for the homogeneous model for the SCALE sensitivity and uncertainty analysis.

Figure 37. SCALE input file for the homogeneous model .

```
'EBR-II Homogeneous Model for TSUNAMI
=tsunami-3d-k6
ebr-ii homogeneous model
ce_v7_endf
read composition
sodium 1 den=0.859 1 666 end
sodium 2 den=0.859 1 666 end
sodium 3 den=0.859 1 666 end
ss316 4 1 685 end
ss316 5 1 685 end
ss316 6 1 685 end
wtpt_emty_drv_rd 10 1.958281 10
11000 23.61659
14000 0.7638035
6000 0.06110428
24000 12.98466
25000 1.527607
26000 49.93365
28000 9.165642
42000 1.909522
2000 0.00306717
15031 0.03435791
1 685 end
wtpt_l_drv_shld 20 6.801966 9
6000 0.07826987
14000 0.9783733
15031 0.0440268
24000 16.63235
25055 1.956747
26000 63.96116
28000 11.74048
11000 2.162665
42000 2.445933
1 685 end
wtpt_l_drv_adpt 30 2.341 8
6000 0.056
14000 0.706
15031 0.032
24000 13.407
```

25055 1.411
26000 48.246
28000 6.703
11000 29.439
1 685 end
wtpt_u_drv_shld 40 4.22937 9
6000 0.071388
14000 0.892355
15031 0.040156
24000 15.17004
25055 1.78471
26000 58.33772
28000 10.70826
11000 10.76449
42000 2.230888
1 685 end
wtpt_up_adptr 50 1.344 8
6000 0.032
14000 0.396
15031 0.018
24000 7.522
25055 0.792
26000 27.07
28000 3.761
11000 60.409
1 685 end
'smeared fuel
C-12 90 0 5.84129544E-05 707.6968297 end
C-13 90 0 6.31778572E-07 707.6968297 end
Na-23 90 0 9.22908390E-03 707.6968297 end
Si-28 90 0 2.91083770E-04 707.6968297 end
Si-29 90 0 1.47872752E-05 707.6968297 end
Si-30 90 0 9.75928649E-06 707.6968297 end
P-31 90 0 1.28789200E-05 707.6968297 end
Cr-50 90 0 1.25929767E-04 707.6968297 end
Cr-52 90 0 2.42843007E-03 707.6968297 end
Cr-53 90 0 2.75364460E-04 707.6968297 end
Cr-54 90 0 6.85440647E-05 707.6968297 end
Cr-55 90 0 3.22713770E-04 707.6968297 end
Fe-54 90 0 6.06557026E-04 707.6968297 end
Fe-56 90 0 9.52164811E-03 707.6968297 end
Fe-57 90 0 2.19896381E-04 707.6968297 end
Fe-58 90 0 2.92641751E-05 707.6968297 end
Ni-58 90 0 1.23382315E-03 707.6968297 end
Ni-60 90 0 4.75266478E-04 707.6968297 end
Ni-61 90 0 2.06594975E-05 707.6968297 end

Ni-62 90 0 6.58715381E-05 707.6968297 end
Ni-64 90 0 1.67755404E-05 707.6968297 end
Sr-90 90 0 6.48377595E-05 707.6968297 end
Zr-92 90 0 8.15099649E-05 707.6968297 end
Zr-93 90 0 7.01410024E-05 707.6968297 end
Zr-94 90 0 8.50095219E-05 707.6968297 end
Zr-96 90 0 7.07882127E-05 707.6968297 end
Mo-92 90 0 3.20243393E-04 707.6968297 end
Mo-94 90 0 1.96194590E-04 707.6968297 end
Mo-95 90 0 3.55047878E-04 707.6968297 end
Mo-96 90 0 3.49736587E-04 707.6968297 end
Mo-97 90 0 2.62140050E-04 707.6968297 end
Mo-98 90 0 5.58645050E-04 707.6968297 end
Mo-100 90 0 2.60715033E-04 707.6968297 end
Tc-99 90 0 6.43211990E-05 707.6968297 end
Ru-96 90 0 7.74756788E-05 707.6968297 end
Ru-99 90 0 1.72494620E-04 707.6968297 end
Ru-100 90 0 1.71466014E-04 707.6968297 end
Ru-101 90 0 2.79645796E-04 707.6968297 end
Ru-102 90 0 4.64063657E-04 707.6968297 end
Ru-104 90 0 2.61556273E-04 707.6968297 end
Rh-103 90 0 2.03844125E-04 707.6968297 end
Xe-134 90 0 6.08515732E-05 707.6968297 end
Cs-133 90 0 4.96817464E-05 707.6968297 end
Cs-135 90 0 5.06058942E-05 707.6968297 end
Cs-137 90 0 4.70946913E-05 707.6968297 end
La-139 90 0 4.79153216E-05 707.6968297 end
Ce-142 90 0 4.21301592E-05 707.6968297 end
Nd-148 90 0 1.19523844E-05 707.6968297 end
U-234 90 0 4.55357441E-07 707.6968297 end
U-235 90 0 7.31357088E-03 707.6968297 end
U-236 90 0 7.27517012E-05 707.6968297 end
U-238 90 0 3.75040264E-03 707.6968297 end
Np-237 90 0 8.55228902E-07 707.6968297 end
Pu-236 90 0 1.30714729E-12 707.6968297 end
Pu-238 90 0 9.16813961E-09 707.6968297 end
Pu-239 90 0 2.01484018E-05 707.6968297 end
Pu-240 90 0 6.68735030E-08 707.6968297 end
Pu-241 90 0 1.92315601E-10 707.6968297 end
Am-241 90 0 1.52933667E-12 707.6968297 end
Am-242 90 0 1.88585969E-15 707.6968297 end
Am-243 90 0 5.85279539E-16 707.6968297 end
Cm-242 90 0 5.39759811E-15 707.6968297 end
Cm-243 90 0 3.04968279E-18 707.6968297 end
Cm-244 90 0 2.02221625E-18 707.6968297 end
Cm-245 90 0 3.87527197E-22 707.6968297 end

Cm-246 90 0 2.69832985E-26 707.6968297 end
sodium 88 1 300 end
sodium 99 1 300 end
end composition
read parameter
gen=6500
npg=5000
nsk=500
htm=no
cet=2
cfp=5
end parameter
read geometry
global unit 150
com="driver subassembly - depletion"
'inner hexduct
hexprism 1 2.8067 36.65 0
'outer hexduct
hexprism 2 2.9083 36.65 0
'outer sodium
hexprism 9 2.9464 78 -28
hexprism 10 2.95 79 -29
'upper smeared section
hexprism 11 2.9083 78 36.65
'lower smeared section
hexprism 12 2.9083 0 -28
'smeared fuel region
media 90 1 1
'hexduct
media 4 1 -1 2
'upper smear
media 88 1 11
'lower smear
media 99 1 12
'sodium inside array
media 1 1 9 -2 -11 -12
'sodium outside array
media 1 1 10 -9
boundary 10
end geometry
read bnds
body=10
all=mirror
end bnds
end data
read sams

```
end sams
end
```